

This discussion paper is/has been under review for the journal *Atmospheric Chemistry and Physics (ACP)*. Please refer to the corresponding final paper in *ACP* if available.

**Chemical processing  
of inorganic halogens  
and related species**

W. C. Keene et al.

# Latitudinal variation in the multiphase chemical processing of inorganic halogens and related species over the eastern North and South Atlantic Oceans

W. C. Keene<sup>1</sup>, M. S. Long<sup>1</sup>, A. A. P. Pszenny<sup>2,3,\*</sup>, R. Sander<sup>4</sup>, J. R. Maben<sup>1</sup>,  
A. J. Wall<sup>2,\*\*</sup>, T. L. O'Halloran<sup>1,\*\*\*</sup>, A. Kerkweg<sup>4,\*\*\*\*</sup>, E. V. Fischer<sup>2,\*\*\*\*\*</sup>, and  
O. Schrems<sup>5</sup>

<sup>1</sup>Department of Environmental Sciences, University of Virginia, Charlottesville, VA 22904, USA

<sup>2</sup>Mount Washington Observatory, North Conway, NH 03860, USA

<sup>3</sup>Institute for the Study of Earth, Oceans, and Space, University of New Hampshire, Durham, NH 03824, USA

<sup>4</sup>Air Chemistry Department, Max-Planck Institute of Chemistry, 55020 Mainz, Germany

<sup>5</sup>Alfred Wegener Institute for Polar and Marine Research, 27515 Bremerhaven, Germany

Title Page

Abstract

Introduction

Conclusions

References

Tables

Figures

◀

▶

◀

▶

Back

Close

Full Screen / Esc

Printer-friendly Version

Interactive Discussion



**Chemical processing  
of inorganic halogens  
and related species**

W. C. Keene et al.

[Title Page](#)[Abstract](#)[Introduction](#)[Conclusions](#)[References](#)[Tables](#)[Figures](#)[I◀](#)[▶I](#)[◀](#)[▶](#)[Back](#)[Close](#)[Full Screen / Esc](#)[Printer-friendly Version](#)[Interactive Discussion](#)

\* now at: Atmospheric Chemistry Program, National Sciences Foundation, Arlington, VA, USA

\*\* now at: Department of Geosciences, Pennsylvania State University, University Park,  
PA 16802, USA

\*\*\* now at: Department of Forest Ecosystems and Society, Oregon State University, Corvallis,  
OR 97330, USA

\*\*\*\* now at: Institute for Atmospheric Physics, University of Mainz, 55020 Mainz, Germany

\*\*\*\*\* now at: Department of Atmospheric Sciences, University of Washington, Seattle,  
WA 98195, USA

Received: 30 March 2009 – Accepted: 2 May 2009 – Published: 14 May 2008

Correspondence to: W. C. Keene (wck@virginia.edu)

Published by Copernicus Publications on behalf of the European Geosciences Union.

## Abstract

Volatile inorganic and size-resolved particulate Cl- and Br-species were measured in near-surface air over a broad range of conditions within four distinct regimes (European – EURO, North African – N-AFR, the Intertropical Convergence Zone – ITCZ, and South Atlantic – S-ATL) along a latitudinal gradient from 51° N to 18° S through the eastern Atlantic Ocean. Processes within each regime were interpreted in conjunction with box-model calculations. Median dry-deposition fluxes of sea salt, oxidized N, and oxidized non-sea-salt S varied by factors of 25, 17, and 9, respectively, among the regimes. Sea-salt production was the primary source for inorganic Cl and Br. Acidification and dechlorination of sea salt primarily by HNO<sub>3</sub> sustained HCl mixing ratios ranging from medians of 82 (ITCZ) to 682 (EURO) pmol mol<sup>-1</sup>. Aerosol pHs inferred from HCl phase partitioning with super-μm size fractions (~3 for EURO to the low 4s for ITCZ) were similar to modeled values. Within all regimes, the dominant sources for atomic Cl were BrCl photolysis and ClO+NO. Maxima in atomic Cl ranged from 2.1 to 7.8×10<sup>4</sup> cm<sup>-3</sup> in the ITCZ and N-AFR regimes, respectively. Because SO<sub>2</sub> solubility over the aerosol pH range was low, S(IV) oxidation by hypohalous acids was unimportant under most conditions. Measured particulate Br<sup>-</sup> (median enrichment factor=0.25) was greater and volatile inorganic Br less than simulated values. Reaction with atomic Br was an important sink for O<sub>3</sub> (5% in EURO to 46% in N-AFR). Formation of halogen nitrates accelerated the oxidation of NO<sub>x</sub> (NO+ NO<sub>2</sub>) primarily via hydrolysis reactions involving S aerosol. Relative to simulations with no halogens, lower NO<sub>x</sub> coupled with direct reactions involving halogens yielded lower OH (by 20% to 54%) in all regimes. Halogen chemistry resulted in net O<sub>3</sub> destruction and steady-state mixing ratios that were lower by 22% (EURO) to 62% (N-AFR) relative to “no-halogen” runs.

## Chemical processing of inorganic halogens and related species

W. C. Keene et al.

Title Page

Abstract

Introduction

Conclusions

References

Tables

Figures

◀

▶

◀

▶

Back

Close

Full Screen / Esc

Printer-friendly Version

Interactive Discussion



## 1 Introduction

Chemical reactions involving inorganic halogens significantly influence the composition of the Earth's atmosphere. The importance of these reactions was first recognized in connection with stratospheric ozone loss, especially within the polar vortices during spring (e.g., Wennberg et al., 1994). In the troposphere, the multiphase processing of reactive halogens significantly modifies conventional HO<sub>x</sub>/NO<sub>x</sub> photochemistry over Arctic and Antarctic sea ice (Foster et al., 2001; Simpson et al., 2007), salt flats (Matveev et al., 2001), coastal cities (Finley and Saltzman, 2006; Osthoff et al., 2008), polluted coastal regions (Pszenny et al., 2007; Pechtl and von Glasow, 2007), and coastal-marine macroalgal beds (Alicke et al., 1999). Modeling studies and observations suggest that transformations involving reactive halogens in the marine boundary layer (MBL) over the open ocean are potentially of much greater global significance in terms of the processing and lifetimes of climatically important gases (e.g., von Glasow et al., 2002a, b; Read et al., 2008; Lawler et al., 2009).

The primary source of reactive inorganic Cl and Br in marine air is the production of sea-salt aerosols by waves breaking at the sea surface (Keene et al., 1999; Sander et al., 2003; respectively) whereas the major sources of reactive I include emission of biogenic iodocarbons from the ocean surface and, in coastal regions, from exposed macroalgae at low tide (Carpenter, 2003); direct emissions of I<sub>2</sub> from macroalgae may also be important (Saiz-Lopez and Plane, 2004). The multiphase photochemical processing of marine-derived halogens influences oxidation capacity through an interrelated set of reactions including catalytic O<sub>3</sub> destruction (Dickerson et al., 1999; Nagao et al., 1999; Galbally et al., 2000; Read et al., 2008); net O<sub>3</sub> production in polluted regions (Tanaka et al., 2003; Osthoff et al., 2008); oxidation of CH<sub>4</sub> (Platt et al., 2004), non-methane hydrocarbons (NMHCs, Wingenter et al., 1996; Pszenny et al., 2007), and (CH<sub>3</sub>)<sub>2</sub>S (Toumi, 1994; Keene et al., 1996; Saiz-Lopez et al., 2004) in the gas phase; oxidation of S(IV) in aerosol solutions (Vogt et al., 1996); and modification of HO<sub>x</sub> (Stutz et al., 1999; Bloss et al., 2005) and NO<sub>x</sub> cycles (Sander et al.,

### Chemical processing of inorganic halogens and related species

W. C. Keene et al.

Title Page

Abstract

Introduction

Conclusions

References

Tables

Figures

◀

▶

◀

▶

Back

Close

Full Screen / Esc

Printer-friendly Version

Interactive Discussion



1999; Pszenny et al., 2004). The associated production of soluble reaction products contributes to aerosol growth. Reactions involving iodine oxides have also been linked to significant nucleation of new particles in some coastal regions (e.g., O'Dowd et al., 2002) (but not others, Russell et al., 2007) suggesting the possibility that similar pathways may operate over the open ocean. Finally, the phase partitioning of HCl regulates the pH of marine aerosol solutions and important associated pH-dependent pathways including halogen activation and S(IV) oxidation (Keene et al., 1998, 2004). Despite its potential importance of reactive halogen chemistry, comprehensive multiphase observations over a broad range of tropospheric conditions, and particularly over the open ocean, are scarce thereby constraining our ability to reliably predict associated influences on O<sub>3</sub> cycling, oxidation processes, aerosol evolution, and radiative transfer regionally and globally. This limitation motivated the investigation reported herein.

## 2 Methods

### 2.1 Cruise track and shipboard sampling

15 During an October and November 2003 cruise of the German research ship *Polarstern* from Bremerhaven, Germany to Cape Town, South Africa (designated cruise number ANT XXI/1), a comprehensive suite of reactive trace gases, size-resolved and bulk aerosol composition, and related meteorological conditions was measured in near-surface air over the eastern Atlantic Ocean along a latitudinal transect from 51.4° N to 17.8° S (Fig. 1). Air was sampled from the top of a walk-up aluminum scaffold mounted above the navigation bridge approximately 5 m port of the ship's center line (schematics of the ship are available on the web at <http://www.awi.de/en/infrastructure/ships/polarstern/>; also see supplementary material, Fig. S1 <http://www.atmos-chem-phys-discuss.net/9/11889/2009/acpd-9-11889-2009-supplement.pdf>). Inlets were positioned approximately 23 m  
25 above the water line. All sampling was suspended during two large, multi-day storm

## Chemical processing of inorganic halogens and related species

W. C. Keene et al.

Title Page

Abstract

Introduction

Conclusions

References

Tables

Figures

◀

▶

◀

▶

Back

Close

Full Screen / Esc

Printer-friendly Version

Interactive Discussion



events (from 43.4° N to 32.8° N and from 17.8° S to the end of the cruise) during which strong winds, bow spray, and/or heavy rain precluded contamination-free sampling. Aerosol sampling was also suspended intermittently during periods of scattered precipitation.

## 2.2 Measurements

### 2.2.1 Reactive trace gases

Water-soluble, volatile inorganic Cl and NO<sub>3</sub> (dominated by and hereafter referred to as HCl and HNO<sub>3</sub>, respectively), NH<sub>3</sub>, HCOOH, and CH<sub>3</sub>COOH were sampled over 2-hour intervals at nominal flow rates of 20 L min<sup>-1</sup> with tandem mist chambers, each of which contained 20 ml deionized water (Keene et al., 2007a). All air volumes reported herein are normalized to standard temperature and pressure (0°C, 1 atm). To minimize artifact phase changes caused by mixing chemically distinct aerosol size fractions on bulk prefilters, air was sampled through a size-fractionating inlet that inertially removed super-μm aerosols from the sample stream. Sub-μm aerosol was removed downstream by an in-line 47-mm Teflon filter (Zefluor 2-μm pore diameter). Samples were analyzed on site by ion chromatography (IC) usually within a few hours after recovery. Collection efficiencies for all species were greater than 95%, precisions based on paired measurements averaged ±10% to ±25%, and corresponding detection limits (DLs; estimated following Keene et al. (1989) for both mist chamber and aerosol samples) ranged from 2 to 23 pmol mol<sup>-1</sup>.

Inorganic Cl gases were sampled in parallel through an identical inlet with a paired set of similar tandem mist chambers samplers (Keene et al., 1993, 2007a; Maben et al., 1995; Pszenny et al., 2004). One sampler was configured with an upstream chamber containing acidic solution [37.5 mM H<sub>2</sub>SO<sub>4</sub> and 0.042 mM (NH<sub>4</sub>)<sub>2</sub>SO<sub>4</sub>], which removed HCl quantitatively but efficiently passed other forms of volatile Cl, and a downstream chamber containing alkaline solution [30.0 mM NaHCO<sub>3</sub> and 0.408 mM NaHSO<sub>3</sub>], which sampled Cl\* (including Cl<sub>2</sub> and HOCl). The other system contained tandem

## Chemical processing of inorganic halogens and related species

W. C. Keene et al.

Title Page

Abstract

Introduction

Conclusions

References

Tables

Figures

◀

▶

◀

▶

Back

Close

Full Screen / Esc

Printer-friendly Version

Interactive Discussion



**Chemical processing  
of inorganic halogens  
and related species**

W. C. Keene et al.

[Title Page](#)[Abstract](#)[Introduction](#)[Conclusions](#)[References](#)[Tables](#)[Figures](#)[◀](#)[▶](#)[◀](#)[▶](#)[Back](#)[Close](#)[Full Screen / Esc](#)[Printer-friendly Version](#)[Interactive Discussion](#)

chambers, both of which contained alkaline solution to sample total volatile inorganic Cl ( $Cl_t$ ). Available evidence (Keene et al., 1993; Maben et al., 1995) indicates that this sampling technique reliably discriminates volatile inorganic Cl from Cl associated with both particles and organic gases and that it quantitatively differentiates between HCl and other forms of volatile inorganic Cl. However, the speciation of  $Cl^*$  cannot be determined unequivocally. Mist solutions were analyzed on site by IC. Precision for both  $Cl^*$  and  $Cl_t$  was  $\pm 15\%$  or  $\pm 12 \text{ pmol Cl mol}^{-1}$ , whichever was the greater absolute value, and the corresponding DL for both was  $24 \text{ pmol Cl mol}^{-1}$ .

Total volatile inorganic Br ( $Br_t$ ) and  $SO_2$  were sampled at a nominal rate of  $80 \text{ L min}^{-1}$  over discrete daytime and nighttime periods using a filterpack technique (Pszenny et al., 2004). An open-face, three-stage, 47-mm-diameter, polycarbonate filterpack housing was loaded with a quartz-fiber (Pallflex 2500 QAT-UP) particle filter followed by tandem rayon filters (Schleicher and Schuell 8S) impregnated with a solution of 10%  $K_2CO_3$  and 10% glycerol (Bardwell et al., 1990). Based on independent analysis of the tandem filters, collection efficiencies for the upstream filter averaged 85% for both analytes. Filterpacks were cleaned, dried, loaded, and unloaded in a class 100 clean bench configured with impregnated filters on the inlet to remove alkaline- and acidic-reactive trace gases. Exposed filters were transferred to polypropylene tubes, stored in glass jars, frozen, and express shipped from Cape Town to Mount Washington Observatory (MWO) where they were analyzed by IC. The average precision for  $Br_t$  was  $\pm 5\%$  or  $\pm 0.05 \text{ pmol Br mol}^{-1}$ , whichever was the greater absolute value, and the corresponding DL was  $0.10 \text{ pmol Br mol}^{-1}$ . The average precision for  $SO_2$  was  $\pm 8\%$  or  $\pm 0.5 \text{ pmol mol}^{-1}$ , whichever was greater, and the corresponding DL was  $1.0 \text{ pmol mol}^{-1}$ .

### 2.2.2 Aerosols

Ambient aerosols were sampled over discrete daytime and nighttime intervals using a modified Graseby-Anderson Model 235 cascade impactor configured with a Liu-Pui

type inlet, precleaned polycarbonate substrates, and quartz-fiber backup filters (Pallflex 2500 QAT-UP) (Pszenny et al., 2004; Keene et al., 2007a). At an average sampling rate of  $0.78 \text{ m}^3 \text{ min}^{-1}$ , the average 50% aerodynamic cut diameters for the impaction stages were 20, 11, 4.3, 2.5, 1.2, and  $0.65 \mu\text{m}$  yielding average geometric mean diameters (GMDs) for the size-resolved samples of 29, 15, 7.0, 3.3, 1.8, 0.89, and  $0.46 \mu\text{m}$ . Bulk aerosol was sampled in parallel on quartz-fiber filters at an average flow rate of  $1.1 \text{ m}^3 \text{ min}^{-1}$ . Impactors and bulk-filter cassettes were cleaned, dried, loaded, and unloaded in a Class 100 clean bench configured as described above. Exposed substrates and filters were halved, transferred to polypropylene tubes, sealed in glass mason jars, frozen, and express shipped from Cape Town to MWO for analysis.

Half sections of each substrate were extracted in 13 ml deionized water using a mini vortexer and sonication; half sections of exposed backup and bulk filters were similarly extracted in 40 ml deionized water. One set of the substrate and filter extracts was analyzed by IC for total (ionized+undissociated)  $\text{Cl}^-$ ,  $\text{Br}^-$ ,  $\text{SO}_4^{2-}$ ,  $\text{CH}_3\text{SO}_3^-$ ,  $\text{HCOO}^-$ ,  $\text{CH}_3\text{COO}^-$ ,  $\text{C}_2\text{O}_4^{2-}$ ,  $\text{NO}_3^-$ ,  $\text{NH}_4^+$ ,  $\text{Na}^+$ ,  $\text{K}^+$ , and  $\text{Mg}^{2+}$  (Keene et al., 2004). Precision for total  $\text{HCOO}^-$ ,  $\text{CH}_3\text{COO}^-$ , and  $\text{Br}^-$  averaged  $>\pm 100\%$  (i.e., most concentrations were less than DLs); precision for  $\text{CH}_3\text{SO}_3^-$  and  $\text{C}_2\text{O}_4^{2-}$  averaged  $\pm 15\%$  to  $\pm 20\%$ ; precision for other analytes averaged about  $\pm 10\%$ .

Internal losses of super- $\mu\text{m}$  aerosols within slotted cascade impactors of this type average about 25% to 30% (e.g. Willeke et al., 1975); other sources of bias for size-resolved particulate analytes based on the above procedures are generally unimportant (Keene et al., 1990). Sea-salt and non-sea-salt (nss) constituents were differentiated using  $\text{Na}^+$  as the reference species (Keene et al., 1986). Departures from sea-salt composition are reported as both absolute deficits and enrichment factors (EFs) relative to sea salt (e.g., Sander et al., 2003). Because they are not conservative in bulk samples, data for particulate  $\text{Cl}^-$  (including measured, sea-salt, and nss concentrations as well as corresponding deficits and EFs relative to sea salt),  $\text{NO}_3^-$ , and  $\text{NH}_4^+$  reported herein and/or used to parameterize model calculations are based on values summed over the size fractions for individual impactor samples. With the exception

## Chemical processing of inorganic halogens and related species

W. C. Keene et al.

Title Page

Abstract

Introduction

Conclusions

References

Tables

Figures

◀

▶

◀

▶

Back

Close

Full Screen / Esc

Printer-friendly Version

Interactive Discussion



of size-resolved concentrations and EFs for  $\text{Br}^-$ , data for particulate  $\text{Br}^-$  (including measured, sea-salt, and nss concentrations as well as corresponding deficits and EFs relative to sea salt),  $\text{Na}^+$ , and nss  $\text{SO}_4^{2-}$  are based on bulk samples.

### 2.2.3 Meteorological conditions and ancillary data

5 Air and sea-surface temperature, relative humidity (RH), pressure, and wind speed and direction were measured continuously with instruments maintained by the ship's crew and compiled as one-minute averages (posted at <http://dship.awi.de/polarstern/index.htm>). Temperature and RH were periodically measured in parallel with a sling psychrometer operated adjacent to the inlets for our samplers; results were statistically indistinguishable from those reported by the ship.  $\text{O}_3$  and CO were measured  
10 continuously by the University of York and compiled as 10-min averages (Carpenter, University of York, unpublished data, 2008). MBL depth was estimated from 1) profiles of virtual potential temperature derived from rawinsondes launched from the ship at 12 Z on most days and at other times on some days, 2) the lowest cloud base measured by a ceilometer operated by the ship's crew, and 3) either the first significant  
15 drop in back scatter or the lowest cloud layer detected with a lidar operated during the cruise (Immler and Schrems, 2006).

### 2.3 Atmospheric transport

Large-scale atmospheric transport was evaluated using both HYbrid Single-Particle Lagrangian Integrated Trajectories (HYSPLIT, Fig. 1) (Draxler et al., 2005) and Lagrangian particle dispersion (FLEXPART) retroplumes (Stohl et al., 2005). Trajectories were initialized at 500 and 1000 m above the sea surface. Samples were classified into four major transport regimes (described in more detail below) based on visual inspection of the back trajectories, the corresponding column and footprint residence time  
20 components of the retroplumes, and local meteorology (Fischer et al., 2006). Samples collected at transitions between regimes were assigned to the regime that corre-

## Chemical processing of inorganic halogens and related species

W. C. Keene et al.

Title Page

Abstract

Introduction

Conclusions

References

Tables

Figures

◀

▶

◀

▶

Back

Close

Full Screen / Esc

Printer-friendly Version

Interactive Discussion



sponded to the greater fraction of sampling time. The regimes are broadly characterized as European influenced (hereafter referred to as EURO), North African influenced (N-AFR), the inter-tropical convergence zone (ITCZ), and South-Atlantic influenced (S-ATL). Start and stop dates, times, and positions for each regime are listed in Table 1.

## 2.4 Calculations

Aerosol pH was inferred from the measured phase partitioning and associated thermodynamic properties (Henry's Law and dissociation constants) of HCl, meteorological conditions (RH and temperature), and hygroscopicity models of aerosol liquid water content (LWC) (Keene et al., 2004). Dry-deposition fluxes of size-resolved particulate-phase species to the surface ocean were modeled based on the measured chemical composition and GMD for each size fraction, wind velocity, air temperature, and RH following Hummelshøj et al. (1992). The laminar sublayer was assumed to be at 98% RH (Lewis and Schwartz, 2004) and the corresponding GMD for each size fraction within the sublayer was based on the measured ionic composition and hygroscopicity models (the same as those used to estimate aerosol LWC in the overlying air; see above). At steady state in the absence of precipitation, dry-deposition fluxes of sea-salt aerosol are balanced by the corresponding emission fluxes. Emission fluxes of particulate  $\text{Cl}^-$  and  $\text{Br}^-$  associated with sea-salt aerosol were inferred from the calculated dry-deposition fluxes of sea-salt  $\text{Na}^+$  and the corresponding concentration ratios in surface seawater (Keene et al., 2007a). Dry-deposition fluxes of HCl,  $\text{Br}_t$ ,  $\text{HNO}_3$ ,  $\text{NH}_3$ , and  $\text{SO}_2$  to the surface ocean were calculated based on the measured mixing ratios, wind speed, air temperature, and surface-ocean-water temperature following Valigura (1995). This approach assumes that the surface ocean is substantially undersaturated with respect to the gas phase and, thus, solubility does not limit corresponding dry-deposition fluxes. We also assume no vertical gradients in particulate- and gas-phase species between the reference height for these approaches (10 m) and the measurement height.

## Chemical processing of inorganic halogens and related species

W. C. Keene et al.

Title Page

Abstract

Introduction

Conclusions

References

Tables

Figures

◀

▶

◀

▶

Back

Close

Full Screen / Esc

Printer-friendly Version

Interactive Discussion



## 2.5 Photochemical-box-model simulations

Chemical processes corresponding to each of the four major transport regimes were simulated with the photochemical box model MECCA (Model Efficiently Calculating Chemistry of the Atmosphere) using the Rosenbrock 3 positive-definite solver (Sander et al., 2005; Sandu and Sander, 2006). MECCA contains a comprehensive atmospheric reaction mechanism that includes transformations involving: 1)  $O_3$ ,  $CH_4$ ,  $HO_x$ , and  $NO_x$ ; 2) non-methane hydrocarbons (NMHCs); 3) halogens (Cl, Br, I); and 4) sulfur. Because iodine species were not measured during the cruise, the iodine mechanism was switched off for these simulations. In addition to gas-phase reactions, the scheme includes fully integrated multiphase transformations involving both aqueous-phase and heterogeneous pathways. Unlike previous versions of MECCA which considered only two aerosol size bins, a recent model version (Sander, unpublished manuscript, 2009) was used in this study to simulate multiple aerosol size bins. Mass transfer is calculated dynamically and does not assume Henry's Law equilibrium conditions (see supplementary material (<http://www.atmos-chem-phys-discuss.net/9/11889/2009/acpd-9-11889-2009-supplement.pdf>), Table S1 for a complete description of the chemical scheme). Photochemical reaction rates vary as a function of solar zenith angle under clear-sky conditions. For each simulation, the model was parameterized based on median values for measurements associated with the corresponding transport regime (Table 2). To minimize sources of variability among results for different regimes, MBL depth for each simulation was set to the median value for the entire cruise. For species that were not measured, reasonable values were assumed. In all simulations, we also assumed a constant  $O_3$  entrainment flux from the free troposphere of  $5 \times 10^{10}$  molecules  $cm^{-2} s^{-1}$  (Thompson and Zafiro, 1983).

The model was initialized with externally mixed populations of unreacted sea salt and pre-existing nss S aerosols. The number ( $N=7$ ) and sizes of sea-salt bins (Table 2) in the model corresponded to the size fractions sampled by the impactor. A single additional bin (diameter=0.18  $\mu m$ ) contained all preexisting nss S. The liquid water content,

### Chemical processing of inorganic halogens and related species

W. C. Keene et al.

Title Page

Abstract

Introduction

Conclusions

References

Tables

Figures

◀

▶

◀

▶

Back

Close

Full Screen / Esc

Printer-friendly Version

Interactive Discussion



salinity, and lifetime against dry deposition for each aerosol size bin were calculated off-line. Dry-deposition velocities for gas-phase species were also calculated off-line. Size-resolved emission fluxes of sea salt for each regime were set equal to the corresponding median values for size-resolved dry-deposition fluxes thereby maintaining constant concentrations and size distributions of conservative particulate-phase constituents during each simulation. At each time step, reacted aerosol was removed from, and an equivalent amount of fresh aerosol was added to, each bin in proportion to the corresponding lifetime of aerosol within that bin.

Vertical profiles of sea salt within the MBL vary as a function of particle size and, thus, the atmospheric lifetimes of sea-salt aerosol within each size bin varied as a function of the corresponding vertical mixing potential (e.g., Lewis and Schwartz, 2004). Consequently, the height to which particles are mixed must be considered explicitly to properly parameterize turnover rates of size-resolved aerosols within the 0-D domain. For each regime, the steady-state vertical profiles of size-resolved sea salt mass within each size bin were estimated assuming neutrally stable conditions based on a power-law relationship (Lewis and Schwartz, 2004) parameterized for the corresponding median meteorological conditions and size-resolved concentrations measured at 23 m (Table 2). Coefficients were calculated to scale near-surface measurements of size-resolved aerosols to mean concentrations over the vertical profiles (Table 2). The liquid water content of each size bin at 23 m was multiplied by the corresponding scaling coefficient to yield a column-averaged value. The atmospheric lifetime against dry deposition for each bin was then calculated directly (column-averaged value/dry-deposition rate). The atmospheric lifetime of the size bin containing preexisting  $\text{SO}_4^{2-}$  was assumed equal to that of the smallest sea-salt size bin. We note that, relative to predictions based on theoretical considerations (Lewis and Schwartz, 2004), the limited available measurements of vertical profiles in bulk sea-salt mass (Blanchard et al., 1984; Maring et al., 2003) indicate substantially greater vertical gradients within the MBL. If these measured profiles are generally representative of conditions within the MBL along the cruise track, turnover rates for sea salt and associated reaction products

**Chemical processing  
of inorganic halogens  
and related species**

W. C. Keene et al.

[Title Page](#)[Abstract](#)[Introduction](#)[Conclusions](#)[References](#)[Tables](#)[Figures](#)[⏪](#)[⏩](#)[◀](#)[▶](#)[Back](#)[Close](#)[Full Screen / Esc](#)[Printer-friendly Version](#)[Interactive Discussion](#)

in the model calculations were underestimated.

At each time step, a mixture of  $\text{HNO}_3$  and  $\text{NO}_2$  was added to the system at a combined rate equal to the corresponding median loss rate of oxidized N ( $\text{HNO}_3$ +particulate  $\text{NO}_3^-$ , hereafter referred to as total  $\text{NO}_3$ ) via dry deposition (calculated from measurements as described in Sect. 2.4). Although the total exogenous source flux of oxidized N was reasonably well constrained by the corresponding dry-deposition fluxes, the relative amounts of  $\text{HNO}_3$  to  $\text{NO}_x$  in the source varied spatially along the cruise track in response to variability in the relative importance of distinct and poorly characterized processes.  $\text{NO}_x$  and  $\text{HNO}_3$  within the MBL have relatively short lifetimes (less than one to two days) against oxidation and deposition, respectively, and, consequently, the importance of transport within the MBL as a source for oxidized N from continental sources decreases rapidly with distance from coasts (e.g., Neuman et al., 2006). Potentially important sources for oxidized N in the more remote open-ocean MBL along the cruise track include entrainment of a time-varying mixture of combustion-and lightning-derived  $\text{HNO}_3$  and  $\text{NO}_x$  from the free troposphere (Neuman et al., 2006; Shepon et al., 2007), direct emissions of NO from ships at sea (Corbett et al., 1999), transport and thermal decomposition of  $\text{NO}_x$  reservoir species such as peroxyacetyl nitrate (PAN) (Jacobi et al., 1999), and chemical degradation of alkyl nitrates emitted from the surface ocean (Dahl et al., 2005). Because spatial variability in the speciation and relative importance of different sources along the cruise track could not be evaluated explicitly, the model was parameterized by adjusting the  $\text{HNO}_3$ : $\text{NO}_2$  ratio in the oxidized N source term for each regime such that corresponding simulated steady-state mixing ratios of  $\text{NO}_x$  fell within the range of available measurements in the eastern Atlantic MBL (e.g., Carsey et al., 1997; Leser et al., 2003; Lawler et al., 2009; Lee et al., 2009). Resulting  $\text{HNO}_3$ : $\text{NO}_2$  ratios in the source terms for the EURO (1:1), N-AFR (5:1), ITCZ (1:1), and S-ATL (4:1) regimes yielded steady-state mixing ratios of  $\text{NO}_x$  averaging 171, 31, 8, and 20  $\text{pmol mol}^{-1}$ , respectively, for the model runs that included transformations involving halogens. The implications of this parameterization scheme are discussed below. ( $\text{CH}_3$ )<sub>2</sub>S emissions were based on

**Chemical processing  
of inorganic halogens  
and related species**

W. C. Keene et al.

Title Page

Abstract

Introduction

Conclusions

References

Tables

Figures

◀

▶

◀

▶

Back

Close

Full Screen / Esc

Printer-friendly Version

Interactive Discussion



the WCRP/IGAC emissions inventory (Roelofs et al., 1998).  $\text{SO}_2$  was added at rates such that  $\text{SO}_2 + (\text{CH}_3)_2\text{S}$  inputs equaled the corresponding median losses of total nss S ( $\text{SO}_2 + \text{nss SO}_4^{2-}$ ) via dry deposition for each regime.  $\text{NH}_3$  was added to the system at rates equal to the corresponding median losses of total reduced N ( $\text{NH}_3 + \text{particulate NH}_4^+$ ) via dry deposition for each regime. The above approach sustained essentially constant steady-state concentrations of total reactive N and S during each simulation.

Our analysis focused primarily on two sets of conditions that were simulated for each of the four regimes. One set (hereafter referred to as “with halogens”) included the full suite of transformations involving inorganic Cl and Br species. For the other set (hereafter referred to as “no halogens”), all transformations involving halogens were switched off (i.e.,  $\text{Cl}^-$  and  $\text{Br}^-$  associated with nascent marine aerosols were chemically inert). To achieve steady state conditions for each simulation, the model was run over a period of 110 days preceding the end point of the corresponding observation period within that flow regime. Results from the last several days of each simulation were interpreted. These simulations provide useful insight concerning the underlying processes. As discussed in more detail below, however, some important aspects of the MBL system (including entrainment rates, the sources and photochemical ages of oxidized N, and mixing ratios of halogen radicals and precursors in ambient air) were poorly constrained by observation. In addition, current models do not reproduce some measured characteristics of the multiphase system, which suggests that they are missing some important processes. Finally, these box model calculations do not consider physiochemical dynamics driven with vertical mixing, non-steady-state conditions, or cloud processing. Consequently, the simulated results may not be representative of ambient conditions in some respects.

**Chemical processing  
of inorganic halogens  
and related species**

W. C. Keene et al.

[Title Page](#)[Abstract](#)[Introduction](#)[Conclusions](#)[References](#)[Tables](#)[Figures](#)[⏪](#)[⏩](#)[◀](#)[▶](#)[Back](#)[Close](#)[Full Screen / Esc](#)[Printer-friendly Version](#)[Interactive Discussion](#)

### 3 Results and discussion

#### 3.1 Atmospheric-transport regimes

The EURO regime was associated with northwesterly flow that had recently (less than one day prior to sampling) passed over western Europe (Fig. 1), variable near-surface wind velocities (median=7.3 m s<sup>-1</sup>), and relatively low temperatures (median=11.4°C) and RHs (median=56.1%) (Fig. 2). The N-AFR regime was characterized by more northerly transport with a long (several day) fetch over the eastern North Atlantic Ocean before passing near or over western North Africa prior to sampling, the highest median wind velocity (8.5 m s<sup>-1</sup>), and increasing temperatures (median=23.2°C) and RHs (median=67.6%). The transition from the Northern to Southern Hemisphere through the ITCZ was characterized by shifting air flow from northerly to southerly, low wind velocities (median=3.5 m s<sup>-1</sup>), widely scattered showers, and relatively high temperatures (median=27.0°C) and RHs (median=78.4%). The S-ATL regime was characterized by persistent southeasterly flow with long fetch over the eastern South Atlantic Ocean roughly parallel to the coast of southern Africa, moderate wind velocities (median=8.1 m s<sup>-1</sup>), and decreasing temperatures (median=22.5°C) and RHs (median=77.3%).

#### 3.2 Multiphase MBL composition and processing

The major physiochemical characteristics of MBL air along the cruise track (Figs. 2, 3, Williams et al., 2007) varied substantially among transport regimes as functions of up-wind emissions of precursors, length and duration of fetch over the ocean, associated meteorological drivers (primarily wind velocity and RH), and chemical processing. In the following sections we evaluate the relative influences of these factors on the cycling of inorganic halogens and related species within each regime.

### Chemical processing of inorganic halogens and related species

W. C. Keene et al.

Title Page

Abstract

Introduction

Conclusions

References

Tables

Figures

◀

▶

◀

▶

Back

Close

Full Screen / Esc

Printer-friendly Version

Interactive Discussion



### 3.3 European influenced

The relatively high concentrations of  $\text{HNO}_3$ , particulate  $\text{NO}_3^-$  (Figs. 2e and 3o) and  $\text{SO}_2$  (Fig. 2f) measured in the EURO regime reflect  $\text{NO}$  and  $\text{SO}_2$  emissions from widespread fossil-fuel combustion across western Europe and from heavy ship traffic in the surrounding ocean. Sea-salt concentrations within this regime varied by a factor of 10 (Fig. 2b) in response to the combined influences of variable wind velocity (Fig. 2a), sea state, and fetch (Fig. 1). The acidification of sea-salt aerosol and associated displacement of  $\text{HCl}$  resulted in the highest  $\text{HCl}$  mixing ratios (Figs. 2c, 4a), lowest  $\text{EF}(\text{Cl}^-)$ s (Fig. 2b), and lowest inferred (from  $\text{HCl}$  phase partitioning) aerosol pHs (Fig. 2g) during the cruise.  $\text{HCl}$  concentrations were generally greater than the corresponding deficits relative to sea salt (Fig. 2c), which assuming that sea-salt  $\text{Cl}^-$  was the primary precursor for  $\text{HCl}$  (addressed below), indicates that  $\text{HCl}$  had longer atmospheric lifetimes against deposition than the parent aerosol. All size fractions were significantly dechlorinated; median  $\text{EF}(\text{Cl}^-)$  decreased with decreasing size (Fig. 3k).

Median size distributions of  $\text{Na}^+$ ,  $\text{NO}_3^-$ , nss  $\text{SO}_4^{2-}$ , and pH (Fig. 3i, n, o, and p, respectively), indicate that  $\text{HNO}_3$  partitioned preferentially with the less-acidic, super- $\mu\text{m}$ -diameter, sea-salt size fractions and was the primary source of acidity incorporated into those size fractions. This is consistent with expectations based on both the pH-dependence of its phase partitioning (e.g., Keene et al., 2004) and previously reported aerosol size distributions in near-surface air over the eastern North Atlantic Ocean (e.g., Huebert et al., 1996) and elsewhere. Low concentrations of nss  $\text{SO}_4^{2-}$  compared to  $\text{NO}_3^-$  in super- $\mu\text{m}$  size fractions (Fig. 3n, o) indicate that  $\text{H}_2\text{SO}_4$  was a relatively minor source of acidity for super- $\mu\text{m}$  marine aerosols. Due in part to the rapid turnover of super- $\mu\text{m}$  aerosol and associated  $\text{NO}_3^-$ , the median dry-deposition flux of total  $\text{NO}_3^-$  was approximately four times greater than that of total nss S (Fig. 5).

$\text{Cl}^*$  was generally less than  $50 \text{ pmol mol}^{-1}$  but higher mixing ratios (peaks between 100 and  $213 \text{ pmol mol}^{-1}$ ) were observed during three intervals, two within several hours after sunrise and the other within several hours after sunset (Fig. 2c). However, sys-

## Chemical processing of inorganic halogens and related species

W. C. Keene et al.

Title Page

Abstract

Introduction

Conclusions

References

Tables

Figures

◀

▶

◀

▶

Back

Close

Full Screen / Esc

Printer-friendly Version

Interactive Discussion



tematic diel variability was not evident, which is consistent with past observations and model calculations (Pszenny et al., 2004; Keene et al., 2007a; Pechtl and von Glasow, 2007). The first two intervals of high  $Cl^*$  occurred in parallel with relatively high RHs (65.6% to 68.5%, Fig. 2a) suggesting a possible link between aerosol water content and net  $Cl^*$  production.

Bulk aerosol was significantly depleted in  $Br^-$  relative to seawater ( $EF(Br^-)$  ranged from 0.37 to 0.71; Fig. 2b) but the smallest size fraction was highly enriched (Fig 3l, m). The enrichment of  $Br^-$  in sub- $\mu m$  aerosol in marine regions has been widely reported (e.g., Sander et al., 2003) but the major cause(s) are not understood. Nascent marine aerosols are not enriched in either  $Br^-$  or total Br (organic+ $Br^-$ ) when initially injected into the atmosphere from the ocean surface (Keene et al., 2007b) and, as detailed below, model calculations based on the halogen activation mechanism (e.g., Vogt et al., 1996) do not predict the significant retention of  $Br^-$  in sea-salt aerosol or the accumulation of  $Br^-$  in sub- $\mu m$  aerosol size fractions. These results suggest the possibility that significant concentrations of Br associated with marine aerosol in the EURO region (and elsewhere) may be present as relatively unreactive, perhaps organic compounds that either originate from non-marine sources or are produced by chemical pathways not considered in current models. However, the median estimated emission fluxes of sea-salt  $Br^-$  (and  $Cl^-$ ) were approximately balanced by the corresponding dry-deposition fluxes of total Br ( $Br_t$  and particulate  $Br^-$ ) (and total Cl, HCl+particulate  $Cl^-$ , Fig. 6), which suggests that the production of sea salt was the primary source for inorganic Br and Cl over the eastern Atlantic Ocean. Similar relationships were observed in polluted air along the northeastern US coast (Keene et al., 2007a). In addition, available evidence indicates that the analytical technique used here (ion chromatography) is specific for  $Br^-$  and it is unlikely that simple dilution during extraction or exposure to eluent solutions or separator column resins would convert bromine sequestered in the chemical lattice of relatively inert compounds to  $Br^-$ . Regardless of speciation, the net effect of retaining and/or accumulating significant marine-derived  $Br^-$  in the particulate phase would be to slow production rates of Br-radical precur-

## Chemical processing of inorganic halogens and related species

W. C. Keene et al.

Title Page

Abstract

Introduction

Conclusions

References

Tables

Figures

◀

▶

◀

▶

Back

Close

Full Screen / Esc

Printer-friendly Version

Interactive Discussion



sors and to modify the importance of different pathways in the cycle relative to those predicated by current models. For example, as  $\text{EF}(\text{Br}^-)$  decreases, the importance of  $\text{HOBr} + \text{Cl}^- + \text{H}^+ \rightarrow \text{BrCl} + \text{H}_2\text{O}$  and subsequent transformations increases relative to  $\text{HOBr} + \text{Br}^- + \text{H}^+ \rightarrow \text{Br}_2 + \text{H}_2\text{O}$  (e.g., Vogt et al., 1996; Fickert et al., 1999). Consequently, the nature of this characteristic of the system must be resolved in order to develop a reliable predictive capability for Br-radical chemistry and the associated influences on the evolution of marine air.

$\text{Br}_t^-$  was present at higher concentrations than the corresponding particulate- $\text{Br}^-$  deficit relative to sea salt (Figs. 2d, 7b), which assuming that sea salt was the primary source for total Br, indicates that  $\text{Br}_t^-$  had a longer atmospheric lifetime than the parent aerosol. In addition,  $\text{Br}_t^-$  varied systematically over diel cycles with daytime mixing ratios approximately two times greater those at night (Fig. 2d). In contrast, the corresponding  $\text{Br}^-$  deficits in bulk aerosol exhibited relatively less day-night variability (Fig. 2d).

The simulated steady-state mixing ratios of  $\text{NO}_x$  in the EURO regime for the “with halogens” run averaged  $171 \text{ pmol mol}^{-1}$  over diel cycles (Fig. 8). The corresponding simulated  $\text{NO}_2$  ( $163 \text{ pmol mol}^{-1}$ ) was within the broad range of daily averages for  $\text{NO}_2$  measured in this region by Leser et al. (2003) ( $\sim 20$  to  $1160 \text{ pmol mol}^{-1}$ ). Simulated size distributions of particulate  $\text{NO}_3^-$ , nss  $\text{SO}_4^{2-}$ , and  $\text{Cl}^-$  for the “with halogen” run (Fig. 9) were similar to those based on median values for the measured near-surface concentrations (Fig. 3n, o, j, respectively). The simulated mixing ratios of  $\text{HNO}_3$  ( $495$  to  $575 \text{ pmol mol}^{-1}$ , not shown) overlapped the upper limit for mixing ratios measured within this regime (Fig. 2e, median= $210 \text{ pmol mol}^{-1}$ ). Simulated  $\text{SO}_2$  ( $456$  to  $501 \text{ pmol mol}^{-1}$ , not shown) fell within the upper range of observations (Fig. 2f, median= $390 \text{ pmol mol}^{-1}$ ) and simulated HCl (Fig. 8,  $251$  to  $293 \text{ pmol mol}^{-1}$ ) was less than most observations (Fig. 2c, median= $680 \text{ pmol mol}^{-1}$ ). The differences between simulated and observed  $\text{HNO}_3$  and HCl both in this and other regimes resulted in part from the scaling approach employed to parameterize average aerosol concentrations and turnover rates for the simulations. The relatively lower  $\text{HNO}_3$  and higher HCl measured

## Chemical processing of inorganic halogens and related species

W. C. Keene et al.

Title Page

Abstract

Introduction

Conclusions

References

Tables

Figures

◀

▶

◀

▶

Back

Close

Full Screen / Esc

Printer-friendly Version

Interactive Discussion



in near-surface air reflect local phase partitioning with the greater near-surface aerosol volumes whereas the simulated results correspond to column-averaged conditions.

5 Simulated pHs for size fractions other than the largest and smallest in the “with halogens” run (Fig. 8, 2.5 to 2.9) were consistent with median values inferred from the measured phase partitioning of HCl (Fig. 3p, 2.5 to 3.1). Similar factors contribute to deviations between simulated and observed pHs for largest and smallest size fractions in this and other regimes (see below). The relatively higher simulated pH for the largest size fraction reflects the rapid turnover rates of large aerosols relative to the kinetics of phase change. Freshly produced and aged aerosols were not simulated as external mixtures. The instantaneous mixing of fresh with chemically aged aerosols during each time step sustained substantial undersaturation of the largest size fraction with respect of acidic gases and, thus, higher solution pH relative to smaller super- $\mu\text{m}$  size fractions (e.g., Pszenny et al., 2004). In contrast, pHs inferred from the measured phase partitioning of HCl were based on the assumption of thermodynamic equilibrium and, consequently, inferred pHs for the larger, undersaturated size fractions represent lower limits (Keene et al., 2004). The low (near detection limit)  $\text{Cl}^-$  concentrations associated with sub- $\mu\text{m}$  aerosols (Fig. 3j) contribute to relatively large uncertainties in estimating pHs based on HCl partitioning. In addition, as described below, the model failed to reproduce some features of sub- $\mu\text{m}$  aerosol composition suggesting that it may be missing some important processes. Both factors may contribute to the relatively large differences between inferred versus simulated pHs for the smaller size fractions. The substantially higher simulated pHs (and associated differences in the phase partitioning of  $\text{HNO}_3$ ) in the “with halogens” relative to the “no halogens” runs for this and other regimes (Figs. 8 and 9) reflect the influences of HCl phase partitioning on aerosol solution acidity in the former versus lack thereof in the latter. Acid displacement of HCl by more soluble acids (primarily  $\text{HNO}_3$ ) transfers acidity from the aerosol solution to the gas phase thereby sustaining relatively higher solution pH in the “with halogens” run (e.g., Keene et al., 1998).

25 Simulated  $\text{Cl}^*$  (the sum of volatile Cl species other than HCl) varied from 52 to

---

## Chemical processing of inorganic halogens and related species

W. C. Keene et al.

---

Title Page

Abstract

Introduction

Conclusions

References

Tables

Figures

◀

▶

◀

▶

Back

Close

Full Screen / Esc

Printer-friendly Version

Interactive Discussion



**Chemical processing  
of inorganic halogens  
and related species**

W. C. Keene et al.

Title Page

Abstract

Introduction

Conclusions

References

Tables

Figures

◀

▶

◀

▶

Back

Close

Full Screen / Esc

Printer-friendly Version

Interactive Discussion

100 pmol mol<sup>-1</sup> over diel cycles (Fig. 8). Although the Cl\* measurements did not indicate systematic diel variability, the simulated values were within the range of observations (Fig. 2c). In the model, Cl\* was dominated during the daytime by HOCl and ClNO<sub>3</sub> (peak values of 51 and 21 pmol mol<sup>-1</sup>, respectively, Fig. 8) and at night by Cl<sub>2</sub> and BrCl (peak values of 36 and 15 pmol mol<sup>-1</sup>, respectively, Fig. 8). In close proximity to large urban and industrial emission sources for NO<sub>x</sub>, ClNO<sub>2</sub> produced via the nocturnal reaction N<sub>2</sub>O<sub>5</sub>+Cl<sup>-</sup>→ClNO<sub>2</sub>+NO<sub>3</sub><sup>-</sup> may accumulate in the dark to mixing ratios >1000 pmol mol<sup>-1</sup> (Ostoff et al., 2007). However, NO<sub>x</sub> is efficiently oxidized to HNO<sub>3</sub> and particulate NO<sub>3</sub><sup>-</sup> in marine air and deposited to the surface. Consequently, NO<sub>x</sub> mixing ratios (e.g., Neuman et al., 2006) and the associated nocturnal production of ClNO<sub>2</sub> decrease rapidly over the ocean with distance from sources, consistent with the simulated values reported herein. For example, relative to the EURO runs in which depositional losses of oxidized N were replaced by an aged mixture of HNO<sub>3</sub> and NO<sub>2</sub> in a ratio of 1:1, a sensitivity run in which losses were replaced entirely by freshly emitted NO yielded steady-state NO<sub>x</sub> mixing ratios averaging 237 pmol mol<sup>-1</sup> and a maximum ClNO<sub>2</sub> mixing ratio of 19 pmol mol<sup>-1</sup>, which were factors of 2 and 4 higher, respectively.

Integrated over 24 h, Cl-atom production was dominated by ClO+NO (36%) and the photolysis of BrCl and Cl<sub>2</sub> (25% and 24%, respectively) but the relative importance of different pathways varied over diel cycles. Following sunrise, the photolysis of Cl<sub>2</sub> and BrCl (produced primarily via heterogeneous reactions of hypohalous acids and halide ions) dominated (49% and 32%, respectively). Photolysis of ClNO<sub>2</sub> accounted for less than 1% of Cl-atom production during this period. During midday, ClO+NO was the most important single pathway (48%) with photolysis of HOCl (19%), BrCl (19%) and Cl<sub>2</sub> (10%) accounting for most of the balance. Cl-atom concentrations peaked following sunrise at 4.3×10<sup>4</sup> cm<sup>-3</sup>, remained high through midday, and declined in the late afternoon (Fig. 8). Although the Cl-atom production pathways under steady-state conditions in the EURO regime were not dominated by the autocatalytic recycling of Cl<sub>2</sub> as simulated in aging pollution plumes elsewhere (Petchl and von Glasow, 2007;



Lawler et al., 2009), the absolute concentrations during daytime were similar. At these levels, oxidation by Cl was a significant sink for alkanes in this regime (e.g., Pszenny et al., 2007). For example, reaction with atomic Cl accounted for 24% of simulated CH<sub>4</sub> oxidation within the EURO MBL.

5 Simulated concentrations of particulate Br<sup>-</sup> indicate that all size fractions except the largest were almost completely debrominated (Fig. 9). As discussed above, however, measured distributions reveal large enrichment in the finest size fraction and retention of significant Br<sup>-</sup> in the larger super- $\mu$ m size fractions (Fig. 3l, m). Causes for these differences are unknown. However, the retention and/or accumulation of significant Br<sup>-</sup> in the ambient aerosol (median EF(Br<sup>-</sup>)=0.52) implies that volatile inorganic Br in the model is overestimated, which is consistent with the factor of two higher mixing ratios of simulated Br<sub>t</sub> (daily average=15 pmol mol<sup>-1</sup>, Fig. 8) relative to measured Br<sub>t</sub> (median=7.2 pmol mol<sup>-1</sup>, Fig. 2d) in this regime. In addition, simulated Br<sub>t</sub> exhibited little diel variability (Fig. 8) whereas that in measured Br<sub>t</sub> was marked (Fig. 2d). Causes for these differences in diel behavior are not known. In the model, Br<sub>t</sub> was dominated by BrCl at night and BrNO<sub>3</sub> during the day (maximum mixing ratios of 15 and 14 pmol mol<sup>-1</sup>, respectively, Fig. 8). The primary sources for atomic Br were BrO+NO (50%) and BrCl photolysis (26%).

20 Destruction of O<sub>3</sub> by atomic Br (O<sub>3</sub>+Br→BrO+O<sub>2</sub>) in the model accounted for 5% of the total O<sub>3</sub> sink associated with all major chemical pathways (including photolysis and reaction with NO, NO<sub>2</sub>, OH, HO<sub>2</sub>, and atomic Cl). Reaction with atomic Cl accounted for 3% of the total. Simulated mixing ratios of product BrO (maximum and midday averages of 1.0 and 0.83 pmol mol<sup>-1</sup>, respectively, Fig. 8), were consistent with measurements of BrO (upper limit of ~1 pmol mol<sup>-1</sup>) in this region during a previous cruise of the Polarstern (Leser et al., 2003). At the high NO<sub>x</sub> mixing ratios in this regime, halogen radical recycling in the gas phase and associated O<sub>3</sub> destruction was slowed by the formation of halogen nitrates (i.e., BrO+NO<sub>2</sub>→BrNO<sub>3</sub> competes with BrO+HO<sub>2</sub>→HOBr), which accumulate to significant concentrations (Fig. 8). Reactions involving S aerosol accounted for 91% of the total heterogenous NO<sub>x</sub> sinks (Fig. 10).

## Chemical processing of inorganic halogens and related species

W. C. Keene et al.

Title Page

Abstract

Introduction

Conclusions

References

Tables

Figures

◀

▶

◀

▶

Back

Close

Full Screen / Esc

Printer-friendly Version

Interactive Discussion



**Chemical processing  
of inorganic halogens  
and related species**

W. C. Keene et al.

[Title Page](#)[Abstract](#)[Introduction](#)[Conclusions](#)[References](#)[Tables](#)[Figures](#)[◀](#)[▶](#)[◀](#)[▶](#)[Back](#)[Close](#)[Full Screen / Esc](#)[Printer-friendly Version](#)[Interactive Discussion](#)

Hydrolysis reactions involving  $\text{ClNO}_3$  (53% of total) and  $\text{BrNO}_3$  (27% of total) to produce hypohalous acids and hydrolysis of  $\text{N}_2\text{O}_5$  to produce  $\text{HNO}_3$  (11% of total) were the most important of these pathways. Of those involving sea salt, the reaction of  $\text{ClNO}_3$  (41%) and  $\text{BrNO}_3$  (26%) with  $\text{Cl}^-$  to produce  $\text{Cl}_2$  and  $\text{BrCl}$ , respectively, were most important. Relative to conventional  $\text{HO}_x/\text{NO}_x$  chemistry, pathways involving halogen nitrates accelerate the conversion of  $\text{NO}_x$  to  $\text{HNO}_3$  and particulate  $\text{NO}_3^-$  (Sander et al., 1999; Pszenny et al., 2004). Comparisons between rates of  $\text{NO}_x$  processing (Fig. 10) and corresponding differences in simulated  $\text{NO}_x$  mixing ratios in the “with halogens” versus “no halogen” runs (averages of 171 and 237  $\text{pmol mol}^{-1}$ , respectively, Fig. 8) indicates that under the polluted conditions in the EURO regime, the overall influences of halogens on  $\text{NO}_x$  cycling was significant. Although the peak simulated mixing ratios of OH and  $\text{HO}_2$  were similar in the “with halogens” versus “no halogens” runs (0.11 versus 0.13  $\text{pmol mol}^{-1}$  and 9.2 versus 8.6  $\text{pmol mol}^{-1}$ , respectively, Table 3), chemical pathways involving halogen chemistry led to substantial net  $\text{O}_3$  destruction. Simulated  $\text{O}_3$  mixing ratios averaged over the day for the “with halogens” (49  $\text{nmol mol}^{-1}$ ) versus “no halogens” (average daily of 64  $\text{nmol mol}^{-1}$ ) runs differed by 23% (Fig. 8). We note that simulated  $\text{O}_3$  mixing ratios were outside the range of measured values within the EURO regime (maximum=47  $\text{nmol mol}^{-1}$ ). Two methodological factors may have contributed to these differences. Chemical transformations involving I-containing compounds were not considered in the simulations but may have contributed to net  $\text{O}_3$  destruction (e.g., Read et al., 2008). In addition, the ratio of  $\text{HNO}_3$  to  $\text{NO}_2$  used to replace depositional losses of oxidized N is poorly constrained. Sensitivity runs based on higher ratios than used in the model parameterization yield lower steady state  $\text{O}_3$  mixing ratios.

### 3.3.1 North African influenced

Relative to EURO, the N-AFR regime was characterized by generally higher sea-salt concentrations (Figs. 2b, 3j), similar ranges in particulate  $\text{NO}_3^-$  and nss  $\text{SO}_4^{2-}$  concen-

**Chemical processing  
of inorganic halogens  
and related species**

W. C. Keene et al.

Title Page

Abstract

Introduction

Conclusions

References

Tables

Figures

◀

▶

◀

▶

Back

Close

Full Screen / Esc

Printer-friendly Version

Interactive Discussion

trations, lower  $\text{HNO}_3$  and  $\text{SO}_2$  mixing ratios (Fig. 2e, f and Fig. 3o, p) and higher pHs (Figs. 2g, 3q). We infer that the most of the oxidized N and S originated as primary or secondary combustion products that were transported from western Europe, western Africa, and ships at sea. Acidification and associated dechlorination of marine aerosol primarily by  $\text{HNO}_3$  (Fig. 3n, o) sustained substantial HCl mixing ratios (Fig. 2c).  $\text{EF}(\text{Cl}^-)$  decreased with decreasing particle size (Fig. 3k) and particulate  $\text{Cl}^-$  deficits summed over all size fractions were generally greater than the corresponding HCl mixing ratios (Fig. 2c) suggesting that the atmospheric lifetime of HCl within this regime was somewhat shorter than that of the parent aerosol.

$\text{Cl}^*$  ranged from  $<24$  to  $129 \text{ pmol Cl mol}^{-1}$  and was detected during most sampling intervals north of  $22^\circ \text{ N}$  (Fig. 2c). Higher mixing ratios during this period were generally observed at night although consistent diel variability was not evident. Between  $22$  and  $18^\circ \text{ N}$ ,  $\text{Cl}^*$  was undetectable; an instrumental malfunction precluded quantification through the southern segment of this regime.

The highest concentrations of  $\text{Br}_t$ , the greatest absolute particulate  $\text{Br}^-$  deficits ( $30.1$  and  $18.6 \text{ pmol mol}^{-1}$ , respectively, Fig. 2d), and the highest particulate  $\text{Br}^-$  concentrations, (Fig. 3l) along the cruise track were measured in the N-AFR region. During a previous cruise of the Polarstern, Leser et al. (2003) detected significant  $\text{BrO}$  ( $>1.0$  to  $3.6 \text{ pmol mol}^{-1}$ ) over a 2-day period off North Africa between  $37$  and  $30^\circ \text{ N}$ .  $\text{BrO}$  was generally  $<1 \text{ pmol mol}^{-1}$  to the north and south of this region. The maximum mixing ratio of  $\text{Br}_t$  along the cruise track during 2003 was also measured in this region (Fig. 2d). This coincidence in maxima for  $\text{BrO}$  (Leser et al., 2003) and  $\text{Br}_t$  (Fig. 2d) suggests that  $\text{Br}$ -radical chemistry along the cruise track during October peaks in this latitudinal band.

As in the EURO regime, bulk aerosol was significantly depleted in  $\text{Br}^-$  relative to seawater (Fig. 2b) but the smallest size fraction was highly enriched (Fig. 3l, m). Also, as in EURO,  $\text{Br}_t$  was present in the N-AFR regime at higher concentrations than particulate  $\text{Br}^-$  (Fig. 2d), which suggests that  $\text{Br}_t$  had a longer atmospheric lifetime against dry deposition than the parent aerosol.  $\text{Br}_t$  varied systematically over diel cycles with mixing

ratios during daytime greater those at night (Fig. 2d). In contrast,  $\text{Br}^-$  associated with bulk aerosol exhibited relatively less day-night variability.

Median estimated emission fluxes of sea-salt  $\text{Br}^-$  and  $\text{Cl}^-$  were approximately balanced by the corresponding dry-deposition fluxes of total Br ( $\text{Br}_t$ +particulate  $\text{Br}^-$ ) and total Cl (HCl+particulate  $\text{Cl}^-$ , Fig. 6), which implies that production of marine aerosol was the primary source for inorganic Cl and Br in this regime.  $\text{Br}_t$  and particulate  $\text{Br}^-$  accounted for approximately equal fractions of the median dry flux of total Br whereas particulate  $\text{Cl}^-$  dominated the median dry flux of total Cl.

Simulated steady-state mixing ratios of NO and  $\text{NO}_2$  in the “with halogens” run for the N-AFR regime averaged 3.6 and 27  $\text{pmol mol}^{-1}$ , respectively, over diel cycles (Fig. 8), which were within the ranges of measurements in this region by Carsey et al. (1997) ( $\text{NO}_x$  range: 17 to 69  $\text{pmol mol}^{-1}$ ;  $\text{NO}_x$  median: 31  $\text{pmol mol}^{-1}$ ), Leser et al. (2003) ( $\text{NO}_2$  range: <24 to 462  $\text{pmol mol}^{-1}$ ), Read et al. (2008) (daytime average NO for October and November: 2.7 and 4.5  $\text{pmol mol}^{-1}$ , respectively), Lawler et al. (2009) ( $\text{NO}_x$  range: <14 to 51  $\text{pmol mol}^{-1}$  during May and June), and Lee et al. (2009) (average  $\text{NO}_x$  for October and November: 18.5 and 20.5  $\text{pmol mol}^{-1}$ , respectively). The simulated size distributions of  $\text{NO}_3^-$ , nss  $\text{SO}_4^{2-}$ , and  $\text{Cl}^-$  in the “with halogens” runs (Fig. 9) were similar to the corresponding median values for measured distributions (Fig. 3n, o, j, respectively). The simulated mixing ratios of  $\text{HNO}_3$  (92 to 108  $\text{pmol mol}^{-1}$ , not shown) were greater than measured mixing ratios (Fig. 2e, median=19  $\text{pmol mol}^{-1}$ ). Simulated  $\text{SO}_2$  (389 to 401  $\text{pmol mol}^{-1}$ , not shown) fell within the upper range of observations (Fig. 2f, median=104  $\text{pmol mol}^{-1}$ ), and simulated HCl (Fig. 8, 254 to 289  $\text{pmol mol}^{-1}$ ) fell within the lower range of observations (Fig. 2c, median=350  $\text{pmol mol}^{-1}$ ). With the exception of the largest and smallest size fractions, simulated aerosol pHs for the “with halogens” run (Fig. 8, all 3.7) were similar to median values inferred from the measured phase partitioning of HCl (Fig. 3p, 3.8 to 3.9).

Simulated  $\text{Cl}^*$  mixing ratios (11 to 26  $\text{pmol mol}^{-1}$ ) were within the range of measured  $\text{Cl}^*$  (Fig. 2c) and were dominated during the daytime by HOCl (Fig. 8, peak value of

## Chemical processing of inorganic halogens and related species

W. C. Keene et al.

Title Page

Abstract

Introduction

Conclusions

References

Tables

Figures

◀

▶

◀

▶

Back

Close

Full Screen / Esc

Printer-friendly Version

Interactive Discussion



**Chemical processing  
of inorganic halogens  
and related species**

W. C. Keene et al.

Title Page

Abstract

Introduction

Conclusions

References

Tables

Figures

◀

▶

◀

▶

Back

Close

Full Screen / Esc

Printer-friendly Version

Interactive Discussion



11 pmol mol<sup>-1</sup>) and at night by BrCl (Fig. 8, peak value of 16 pmol mol<sup>-1</sup>). The simulated nocturnal mixing ratios of Cl<sub>2</sub> (maximum of 2.8 pmol mol<sup>-1</sup>) were at the lower limit and BrCl was greater than corresponding measured mixing ratios in aged polluted air at Cape Verde (maximum of 35 and <2 pmol mol<sup>-1</sup>, respectively, Lawler et al., 2009).

5 These differences relate in part to the fact that our model calculations were based on steady-state conditions whereas Lawler et al. (2009) simulate conditions within a chemically evolving pollutant plume. Cl-atom production in our model was dominated by BrCl photolysis (66%) and ClO+NO (24%). Atomic Cl peaked in early morning at concentrations of 7.8×10<sup>4</sup> cm<sup>-3</sup> and remained high throughout the day (Fig. 8). Similar concentrations of atomic Cl were simulated by (Lawler et al., 2009) although the primary precursor under those conditions was Cl<sub>2</sub> sustained by autocatalytic cycling. At these concentrations, atomic Cl was an important oxidant for alkanes and (CH<sub>3</sub>)<sub>2</sub>S and accounted for 36% of simulated CH<sub>4</sub> oxidation in this regime.

15 The simulated size distribution of Br<sup>-</sup> (Fig. 8) differed considerably from measured distributions (Fig. 3l). All simulated size fractions except the largest two were almost completely debrominated. In contrast, measured distributions reveal large enrichment relative to sea salt in the finest size fraction and retention of significant Br<sup>-</sup> in all super-μm size fractions (Fig. 3l, m). As discussed above, causes for these differences are unknown. The median measured EF(Br<sup>-</sup>) (0.25) for bulk aerosol implies that volatile inorganic Br in the model is overestimated. The retention of Br in the aerosol coupled with the high concentrations and rapid turnover of sea salt and the longer lifetime against deposition of Br<sub>t</sub> relative to the parent aerosol contributed to higher mixing ratios of simulated Br<sub>t</sub> (averaging 37 pmol mol<sup>-1</sup> over diel cycles, Fig. 8) compared to measured values (median of 19 pmol mol<sup>-1</sup>, Fig. 2d). In the model, BrCl and Br<sub>2</sub> dominated Br<sub>t</sub> at night (maxima of 16 and 13 pmol mol<sup>-1</sup>, respectively) and HBr, BrNO<sub>3</sub>, and HOBr dominated during the day (maxima of 18, 18, and 11 pmol mol<sup>-1</sup>, respectively). The dominant sources for atomic Br were BrO+NO (31%) and the photolysis of HOBr (21%), Br<sub>2</sub> (19%), and BrCl (18%).

25 Reaction with atomic Br and Cl accounted for 46% and 2% of the total modeled

**Chemical processing  
of inorganic halogens  
and related species**

W. C. Keene et al.

Title Page

Abstract

Introduction

Conclusions

References

Tables

Figures

◀

▶

◀

▶

Back

Close

Full Screen / Esc

Printer-friendly Version

Interactive Discussion



O<sub>3</sub> sink in this regime. Simulated BrO mixing ratios peaked following sunrise at 7.8 pmol mol<sup>-1</sup>. The average simulated mixing ratio during midday (4.7 pmol mol<sup>-1</sup>) was near the upper limits for both long-term measurements of BrO at Cape Verde (day-time average of 2.5 ± 1.1 pmol mol, Read et al., 2008) and measurements within the N-AFR regime during a previous cruise of the Polarstern (less than 3.6 pmol mol<sup>-1</sup>, Leser et al., 2003). The retention/accumulation of Br<sup>-</sup> in the ambient aerosol but not in the model coupled with the longer lifetime of volatile relative to particulate Br contributed to these differences. In addition, the median concentration of total sea salt within this regime during autumn (397 nmol Na<sup>+</sup> m<sup>-3</sup>, Table 2) was substantially greater than reported concentrations at Cape Verde during spring (74 to 254 nmol Na<sup>+</sup> m<sup>-3</sup>, Lawler et al., 2009). This implies that the emission flux of particulate Br<sup>-</sup> associated with sea-salt production and the corresponding mixing ratios of volatile inorganic Br based on median conditions for the N-AFR regime were greater than those at Cape Verde, which would have also contributed to the higher BrO simulated for this regime relative to BrO measured at Cape Verde.

Halogen chemistry accelerated the oxidation of NO<sub>x</sub> to HNO<sub>3</sub> and particulate NO<sub>3</sub><sup>-</sup> relative to rates predicated based on conventional HO<sub>x</sub>/NO<sub>x</sub> chemistry (Fig. 10) yielding substantially lower steady-state NO<sub>x</sub> mixing ratios (daily averages of 31 and 62 pmol mol<sup>-1</sup> for the “with halogens” versus “no halogens” runs, respectively, Fig. 8). Following sunrise, the photolysis of Br<sub>2</sub>, BrCl, and Cl<sub>2</sub> initiated active halogen-radical chemistry and the associated oxidation of NO<sub>x</sub> via production of halogen nitrates and subsequent heterogeneous reactions with aerosols, primarily during early morning. Reactions involving S aerosol accounted for 69% of the total heterogeneous sink with hydrolysis of BrNO<sub>3</sub> and ClNO<sub>3</sub> to produce hypohalous acids accounting for 54% and 14%, respectively, of the total. The subset of reactions involving sea salt was dominated by BrNO<sub>3</sub> + Cl<sup>-</sup> → BrCl + NO<sub>3</sub><sup>-</sup> (60%). Relative to the “with halogens” run, daily maxima in simulated OH and HO<sub>2</sub> in the “no halogens” run (Table 3) were higher by factors of 2.8, and 1.5, respectively. In contrast to these results, Read et al. (2008) report that, when halogen chemistry is not included in their box model calculations

for conditions at Cape Verde, OH is lower by 5% to 12%. However, in the Read et al. (2008) model calculations both with and without halogens, NO is constrained by the same measured mixing ratios. While this approach may have characterized the direct influences of halogens on OH, the large indirect influences on OH resulting from the accelerated oxidation of NO<sub>x</sub> via halogen chemistry (Fig. 10) was not considered explicitly. Model calculations reported herein indicate that, when these indirect influences are included, halogen chemistry leads to a substantial net decrease not increase in OH concentrations under conditions for the N-AFR regime. The lower concentrations of simulated OH and HO<sub>2</sub> in the “with halogen” runs for both this regime and those to the south have important implications for oxidation processes in the MBL and the corresponding atmospheric lifetimes of climatically important trace gases including CH<sub>4</sub>.

The combined interrelated influences of Br and Cl via direct reaction, accelerated oxidation of NO<sub>x</sub>, and shifts in the concentrations and relative abundance of OH and HO<sub>2</sub> yielded simulated O<sub>3</sub> mixing ratios averaging 14 nmol mol<sup>-1</sup> (Fig. 8), which was outside the observed range (45 to 20 nmol mol<sup>-1</sup>) and substantially lower than that for the “no halogens” run (37 pmol mol<sup>-1</sup>, Fig. 8). In addition to the less vigorous multi-phase cycling of ambient relative to simulated Br discussed above, several other factors contributed to differences between measured O<sub>3</sub> versus that simulated in the “with halogens” runs. Rates of O<sub>3</sub> entrainment (an important O<sub>3</sub> source in this region, Read et al., 2008) may be underestimated in the model. The simulations assume clear-sky conditions. Because scattered clouds were present during most of the cruise and attenuated ambient photon fluxes, rates of Br and Cl photochemistry and associated net O<sub>3</sub> destruction in the model corresponded to upper limits. Finally, iodine-radical chemistry is an important sink for O<sub>3</sub> in this region (Read et al., 2008) that was not considered in our simulations. If influences of iodine are excluded, the relative contribution of transformations involving Br to the other major O<sub>3</sub> sinks modeled by Read et al. (2008) for conditions at Cape Verde during March (23%) are a factor of two less than those simulated herein during autumn (46%).

**Chemical processing  
of inorganic halogens  
and related species**

W. C. Keene et al.

Title Page

Abstract

Introduction

Conclusions

References

Tables

Figures

◀

▶

◀

▶

Back

Close

Full Screen / Esc

Printer-friendly Version

Interactive Discussion



### 3.3.2 ITCZ

The relatively low wind velocities within the ITCZ regime (Fig. 2a), perhaps coupled with relatively greater wet removal via the higher frequency of scattered showers, resulted in lowest sea-salt concentrations measured along the cruise track (Figs. 2b, 3o). The lowest concentrations of total  $\text{NO}_3$  (Fig. 2e) and total nss S (Fig. 2f) and corresponding dry-deposition fluxes (Fig. 5) were also observed within this regime. The relatively low HCl mixing ratios (Fig. 2c), high  $\text{EF}(\text{Cl}^-)$ s (Fig. 2b), and high aerosol pHs (Fig. 3q) reflect the low concentrations of acids.  $\text{Cl}^*$  was undetectable during most sampling intervals within this regime (Fig. 2c) but, between  $5^\circ$  and  $2^\circ$  N, nocturnal mixing ratios increased from  $<24 \text{ pmol mol}^{-1}$  to a predawn peak of  $136 \text{ pmol mol}^{-1}$ . This episode coincided with increasing RH (Fig. 2a) and nss  $\text{SO}_4^{2-}$  concentrations (Fig. 2e).

$\text{Br}_f$  and particulate  $\text{Br}^-$  deficits were low relative to those in other regions (Fig. 2d). Based on median values, size-resolved  $\text{EF}(\text{Br}^-)$  was systematically lower than corresponding values for northerly segments of the cruise and, notably, no enrichment was evident in the smallest size fraction (Fig. 3). As in the other regimes, the dry-deposition fluxes of total inorganic Cl and Br were approximately balanced by the corresponding emission flux of  $\text{Cl}^-$  and  $\text{Br}^-$  associated with sea salt (Fig. 5) suggesting that nss sources of inorganic Cl and Br were unimportant.

Simulated steady-state mixing ratios of  $\text{NO}_x$  in the “with halogens” run averaged  $8.3 \text{ pmol mol}^{-1}$  over diel cycles (Fig. 8). The corresponding  $\text{NO}_2$  ( $7.8 \text{ pmol mol}^{-1}$ , not shown) was less than the upper limits estimated by Leser et al. (2003) based on measurements in this region ( $<24$  to  $<100 \text{ pmol mol}^{-1}$ ). The simulated size distributions of nss  $\text{SO}_4^{2-}$ , and  $\text{Cl}^-$  (Fig. 9) were similar to the median measured distributions (Fig. 3o, j, respectively). Although the shapes of the measured and simulated size distributions for  $\text{NO}_3^-$  were similar (Figs. 3n and 9, respectively), the simulated concentrations were greater by a factor of about two. The simulated mixing ratios of  $\text{HNO}_3$  (28 to  $37 \text{ pmol mol}^{-1}$ , not shown) and  $\text{SO}_2$  (57 to  $71 \text{ pmol mol}^{-1}$ , not shown) were also greater than measured values (Fig. 2e, median= $12 \text{ pmol mol}^{-1}$  and Fig. 2f,

## Chemical processing of inorganic halogens and related species

W. C. Keene et al.

Title Page

Abstract

Introduction

Conclusions

References

Tables

Figures

◀

▶

◀

▶

Back

Close

Full Screen / Esc

Printer-friendly Version

Interactive Discussion



**Chemical processing  
of inorganic halogens  
and related species**

W. C. Keene et al.

Title Page

Abstract

Introduction

Conclusions

References

Tables

Figures

◀

▶

◀

▶

Back

Close

Full Screen / Esc

Printer-friendly Version

Interactive Discussion

median=19 pmol mol<sup>-1</sup>, respectively). Scavenging and wet deposition via precipitation was not considered in the model but probably contributed to the relatively lower measured versus simulated concentrations of soluble species in this regime. Simulated HCl (Fig. 8, 16 to 22 pmol mol<sup>-1</sup>) was within the lower range of observations (Fig. 2c, median=82 pmol mol<sup>-1</sup>). Simulated pHs for middle five size fractions in the “with halogens” run (Fig. 8, 3.4 to 3.7) were generally lower than median values inferred from the measured phase partitioning of HCl (Fig. 3p, 3.3 to 4.6).

Simulated Cl\* mixing ratios (20 to 30 pmol mol<sup>-1</sup>, Fig. 8) were within the range of measured Cl\* (Fig. 2c) and dominated by HOCl during daytime (maximum of 21 pmol mol<sup>-1</sup>) and HOCl, BrCl, and Cl<sub>2</sub> at night (maxima of 9.5, 7.0, and 5.3 pmol mol<sup>-1</sup>, respectively, Fig. 8). Photolysis of BrCl and HOCl and ClO + NO were the dominant sources for atomic Cl in the model (62%, 15%, and 16%, respectively), which peaked during midday at concentrations of 2.1×10<sup>4</sup> cm<sup>-3</sup> (Fig. 8). At these concentrations, Cl was an important oxidant for alkanes and account for 48% of the modeled sink for CH<sub>4</sub> in this region.

The simulated size distribution of Br<sup>-</sup> (Fig. 9) was similar to the median for measured distributions (Fig. 3l). Most individual Br<sup>-</sup> concentrations for the impactor samples were below DLs and all simulated size fractions were almost completely debrominated. However, the median measured EF(Br<sup>-</sup>) in bulk aerosol (0.35), for which analytical resolution was better, indicates that significant amounts of Br<sup>-</sup> were retained by or accumulated in ambient aerosol (Fig. 2b). Simulated Br<sub>t</sub> averaged 8.3 pmol mol<sup>-1</sup> over diel cycles, which was greater than all measured values (Fig. 2d; median=2.4 pmol mol). As in the other regimes, retention of Br in the aerosol contributed to lower mixing ratios of measured versus simulated Br<sub>t</sub>. In the model, Br<sub>t</sub> was dominated by BrCl at night (maxima of 7.0 pmol mol<sup>-1</sup>) and BrNO<sub>3</sub>, HOBr, and BrO during the day (maxima of 3.2, 3.2, and 3.0 pmol mol<sup>-1</sup>, respectively, Fig. 8). The primary sources for atomic Br were photolysis of BrCl (38%) and HOBr (24%) and BrO+NO (15%).

Reaction with atomic Br and Cl accounted for 35% and 5%, respectively, of the total chemical sink for O<sub>3</sub> within this regime. However, simulated BrO mixing ratios during



midday (maximum and midday average of 3.0 and 2.5 pmol mol<sup>-1</sup>) were greater than values measured in this regions during a previous cruise (<1 pmol mol<sup>-1</sup>, Leser et al., 2003), which suggests that the simulations may overestimate the influence of Br on O<sub>3</sub>. The accelerated oxidation of NO<sub>x</sub> by halogen chemistry (Fig. 10) yielded substantially lower average steady-state NO<sub>x</sub> mixing ratios (8.3 versus 27 pmol mol<sup>-1</sup>, Fig. 8). Reactions involving S aerosol accounted for 86% of the total heterogenous sink, which was dominated by hydrolysis reactions involving ClNO<sub>3</sub> and BrNO<sub>3</sub> (54% and 33% of the total, respectively). Pathways involving sea salt were dominated by ClNO<sub>3</sub> and BrNO<sub>3</sub> reaction with Cl<sup>-</sup> to produce Cl<sub>2</sub> and BrCl (29% and 21%, respectively) and ClNO<sub>3</sub> and BrNO<sub>3</sub> hydrolysis (24% and 17%, respectively). Relative to the “with halogens” runs, daily maxima in simulated OH and HO<sub>2</sub> in the “no halogens” run (Table 3) were also higher by factors of 1.44 and 1.35, respectively. The combined influences of Br and Cl via direct reaction, accelerated oxidation of NO<sub>x</sub>, and reductions in OH and HO<sub>2</sub> concentrations yielded simulated O<sub>3</sub> mixing ratios averaging 29 nmol mol<sup>-1</sup> (Fig. 8) in good agreement with the median measured value (30 nmol mol<sup>-1</sup>). Simulated O<sub>3</sub> for the “no halogens” run (41 nmol mol<sup>-1</sup>, Fig. 8) was outside the range of measured values (35 to 12 pmol mol<sup>-1</sup>). As for the N-AFR regime, several factors may influence comparability of measured versus simulated O<sub>3</sub> in the “with halogens” run; these including the entrainment flux of O<sub>3</sub>, attenuation of radiation by clouds, sequestering of significant Br in ambient aerosols, and iodine chemistry. In addition, the calculation of the scaling coefficients did not consider the conditional instability of the region which, when corrected for stability, would yield vertical scaling coefficients closer to unity for the larger aerosol size-bins. Simulations (not reported) parameterized with the measured (i.e., non-scaled) aerosol concentrations at 23 m indicate that the modeled results are sensitive to the vertical scaling approach, particularly at the lower wind velocities for this regime, which correspond to relatively greater vertical gradients in sea-salt mass (Table 2).

**Chemical processing  
of inorganic halogens  
and related species**

W. C. Keene et al.

[Title Page](#)[Abstract](#)[Introduction](#)[Conclusions](#)[References](#)[Tables](#)[Figures](#)[◀](#)[▶](#)[◀](#)[▶](#)[Back](#)[Close](#)[Full Screen / Esc](#)[Printer-friendly Version](#)[Interactive Discussion](#)

### 3.3.3 South Atlantic

The S-ATL regime was characterized by increasing  $\text{HNO}_3$ , particulate  $\text{NO}_3^-$  (Fig. 2e), and sea-salt concentrations (Fig. 2b). Relative to the ITCZ, the increasing levels of acidity sustained generally lower  $\text{EF}(\text{Cl}^-)$ s (Fig. 2b) and higher HCl (Fig. 2d). Median inferred pHs for the sea-salt size fractions in this regime were similar to those in the N-AFR regime but pHs for the sub- $\mu\text{m}$  size fractions were lower (Fig. 3p). Median dry-deposition fluxes of total  $\text{NO}_3$  and  $\text{SO}_4$  were lower by factors of 2.1 and 2.7, respectively, than those for N-AFR (Fig. 5) indicating that combustion products were relatively less important in this regime. In addition, and in contrast to other regions,  $\text{SO}_2$  in the S-ATL regime exhibited fairly consistent diel variability with higher mixing ratios during daytime and lower at night (Fig. 2f). This pattern would be consistent with the hypothesis that substantial  $\text{SO}_2$  in this region was produced photochemically during the daytime via oxidation of marine-derived  $(\text{CH}_3)_2\text{S}$  by OH, BrO, and Cl and subsequently lost via a combination of deposition to the surface and oxidation to particulate  $\text{H}_2\text{SO}_4$  through multiphase pathways (e.g., Vogt et al., 1996). Combustion-derived  $\text{SO}_2$  would not be expected to exhibit diel variability of this nature.

Concentrations of both  $\text{Br}_t$  and particulate  $\text{Br}^-$  deficits were generally greater than those in the ITCZ. In contrast to EURO and N-AFR,  $\text{Br}_t$  in the S-ATL regime did not exhibit systematic diel variability.  $\text{EF}(\text{Br}^-)$  was generally less than 0.3 (Fig. 2b) and all size fractions were significantly depleted relative to sea salt (Fig. 3m). During most sampling periods,  $\text{Br}_t$  was present at higher concentrations than the corresponding particulate  $\text{Br}^-$  deficits (Fig. 2d) and dominated the median dry-deposition flux of total inorganic Br (Fig. 6b). In addition, the median emission flux of  $\text{Br}^-$  in association with sea salt was approximately balanced by the corresponding dry deposition of total inorganic Br. These relationships indicate that nascent aerosols were efficiently debrominated under these conditions and that  $\text{Br}_t$  had a longer lifetime against deposition than the parent aerosol.

Simulated steady-state mixing ratios of  $\text{NO}_x$  in the “with halogens” run averaged

## Chemical processing of inorganic halogens and related species

W. C. Keene et al.

Title Page

Abstract

Introduction

Conclusions

References

Tables

Figures

◀

▶

◀

▶

Back

Close

Full Screen / Esc

Printer-friendly Version

Interactive Discussion



**Chemical processing  
of inorganic halogens  
and related species**

W. C. Keene et al.

20 pmol mol<sup>-1</sup> over diel cycles (Fig. 8). The corresponding NO<sub>2</sub> (17 pmol mol<sup>-1</sup>, not shown) was within the range estimated by Leser et al. (2003) based on measurements in this region (<24 to <100 pmol mol<sup>-1</sup>). The simulated size distributions of nss SO<sub>4</sub><sup>2-</sup> and Cl<sup>-</sup> in the “with halogens” runs (Fig. 9) were similar to the corresponding median measured distributions (Fig. 3o, j, respectively). As for the ITCZ, the shape of the simulated size distribution for NO<sub>3</sub><sup>-</sup> (Fig. 8) was similar to measurements (Fig. 3n) but the corresponding concentrations were greater by a factor of about two. The simulated HNO<sub>3</sub> (56 to 65 pmol mol<sup>-1</sup>, not shown) was within the upper range of measured values (Fig. 2e, median=21 pmol mol<sup>-1</sup>). Simulated SO<sub>2</sub> (105 to 121 pmol mol<sup>-1</sup>, not shown), which originated primarily from the oxidation of (CH<sub>3</sub>)<sub>2</sub>S, was outside the range of observations (Fig. 2f, median=23 pmol mol<sup>-1</sup>) and simulated HCl (Fig. 8, 114 to 128 pmol mol<sup>-1</sup>) was within the lower range of observations (Fig. 2c, median=270 pmol mol<sup>-1</sup>). Simulated pHs for the middle five size fractions in the “with halogens” run (Fig. 8, 3.8 to 4.0) were within the range of median values inferred from the measured phase partitioning of HCl (Fig. 3p, 3.5 to 3.9).

Simulated Cl\* mixing ratios (8.3 to 19 pmol mol<sup>-1</sup>) were within the range of measured Cl\* (Fig. 2c) and dominated by HOCl during the day (Fig. 8, maximum of 8.8 pmol mol<sup>-1</sup> and BrCl at night (10 pmol mol<sup>-1</sup>). Cl<sub>2</sub> peaked at 2.0 pmol mol<sup>-1</sup> and contributed significantly to Cl\* before dawn. Photolysis of BrCl and HOCl and ClO+NO were the dominant sources (64%, 11%, and 22%, respectively) for atomic Cl, which peaked during midday at concentrations of 4.1 × 10<sup>4</sup> cm<sup>-3</sup> (Fig. 8). Atomic Cl accounted for 19% of simulated CH<sub>4</sub> oxidation in this regime.

The simulated size distribution of Br<sup>-</sup> (Fig. 8) was similar to the median for measured distributions (Fig. 3l). Most individual Br<sup>-</sup> concentrations for the impactor samples were below DLs and all simulated size fractions except the largest were almost completely debrominated. The median measured EF(Br<sup>-</sup>) for bulk aerosol (0.14) also indicates relatively less Br<sup>-</sup> associated with ambient aerosol compared to other regimes (Fig. 2b). Like the measurements, simulated Br<sub>f</sub> exhibited little diel variability (Fig. 8) but measured mixing ratios (Fig. 2d, median of 6.2 pmol mol<sup>-1</sup>) were substantially lower than

[Title Page](#)[Abstract](#)[Introduction](#)[Conclusions](#)[References](#)[Tables](#)[Figures](#)[◀](#)[▶](#)[◀](#)[▶](#)[Back](#)[Close](#)[Full Screen / Esc](#)[Printer-friendly Version](#)[Interactive Discussion](#)

simulated values (average of  $23 \text{ pmol mol}^{-1}$ ). Retention of  $\text{Br}^-$  in the aerosol coupled with the longer lifetime against deposition for  $\text{Br}_t$  relative to the parent aerosols contributed to these differences.  $\text{Br}_t$  in the model, was dominated by  $\text{BrCl}$  and  $\text{Br}_2$  at night (maxima of 10 and  $6.9 \text{ pmol mol}^{-1}$ , respectively) and  $\text{HBr}$ ,  $\text{BrNO}_3$ , and  $\text{HOBr}$  during the day (maxima of 12, 9.5, and  $7.4 \text{ pmol mol}^{-1}$ , respectively). The primary sources for atomic Br were photolysis of  $\text{HOBr}$  (29%),  $\text{BrCl}$  (19%), and  $\text{Br}_2$  (16%) and  $\text{BrO} + \text{NO}$  (26%).

As in the ITCZ regime, reaction with atomic Br was a significant sink for simulated  $\text{O}_3$  (30%). Simulated  $\text{BrO}$  (maximum and average midday mixing ratios of 6.5 and  $2.8 \text{ pmol mol}^{-1}$ , respectively) was greater than measured values within this region during a previous cruise ( $<1 \text{ pmol mol}^{-1}$ , Leser et al., 2003). As in the other regimes, halogen chemistry accelerated the oxidation of  $\text{NO}_x$  to  $\text{HNO}_3$  and particulate  $\text{NO}_3^-$  relative to rates predicated based on conventional  $\text{HO}_x/\text{NO}_x$  chemistry (Fig. 10) yielding substantially lower steady-state  $\text{NO}_x$  mixing ratios (20 versus  $37 \text{ pmol mol}^{-1}$ , Fig. 8). As in other regimes, reactions involving halogen nitrates and S aerosol dominated (79%) the total heterogeneous sink with the hydrolysis of  $\text{BrNO}_3$  and  $\text{ClNO}_3$  accounting for most of the total (59% and 16%, respectively). Production of  $\text{BrCl}$  via  $\text{BrNO}_3 + \text{Cl}^-$  accounted for 55% of the heterogeneous reactions involving sea salt. Relative to the “with halogens” run, daily maxima in simulated OH and  $\text{HO}_2$  in the “no halogens” run (Table 3) were greater by factors of 1.66 and 1.33, respectively. The combined influences of Br and Cl via direct reaction, accelerated oxidation of  $\text{NO}_x$  and changes in OH and  $\text{HO}_2$  yielded simulated  $\text{O}_3$  mixing ratios averaging  $14 \text{ nmol mol}^{-1}$  (Fig. 8), which were at the lower limit of measured values (14 to  $35 \text{ nmol mol}^{-1}$ ) and a factor of two less than that simulated in the “no halogens” run ( $27 \text{ nmol mol}^{-1}$ , Fig. 8). The same caveats mentioned above regarding comparisons between measured and simulated  $\text{O}_3$  for other regimes apply to the S-ATL.

**Chemical processing  
of inorganic halogens  
and related species**

W. C. Keene et al.

Title Page

Abstract

Introduction

Conclusions

References

Tables

Figures

◀

▶

◀

▶

Back

Close

Full Screen / Esc

Printer-friendly Version

Interactive Discussion



### 3.4 Implications

Simulated results for all regimes are summarized in Table 3. As discussed above, the model reproduced many measured characteristics of the multiphase system with reasonable confidence, which implies that simulated characteristics that were not constrained by observations provide useful insight concerning the underlying physiochemical processes. In addition, when evident, large divergence between simulated and measured values suggest potential problems related to the parameterization scheme for the model and/or limitations in our current understanding of major processes. Relative to the substantial variability in median fluxes and concentrations of sea salt, acidic gases, and precursors and corresponding variability in aerosol pH across the four regimes, simulated maxima for daytime concentrations of atomic Cl varied over a narrow range of 2.1 to  $7.8 \times 10^4 \text{ cm}^{-3}$ . The lowest simulated Cl-atom concentrations were in the ITCZ regime, which contained the lowest median concentrations of sea salt and acids. The highest levels were in the N-AFR regime, which contained the highest concentrations of sea salt but lower levels of combustion products and HCl relative to the EURO regime. The substantial Cl-atom concentrations simulated over this wide range in physiochemical conditions and their consistency with published estimates based on measurements elsewhere (e.g., Pszenny et al., 2007; Lawler et al., 2009; and references therein) supports the hypothesis that Cl-radical chemistry contributes significantly to oxidation potential with implications for the corresponding atmospheric lifetimes of alkanes and  $(\text{CH}_3)_2\text{S}$  within the MBL over broad geographic regions. BrO was also an important oxidant for  $(\text{CH}_3)_2\text{S}$  in the model. For the “with halogens” runs, reaction with atomic Cl and BrO accounted for 6% and 7%, respectively, of  $(\text{CH}_3)_2\text{S}$  oxidation in the EURO regime; 16% and 59%, respectively, in N-AFR; 12% and 72%, respectively, in the ITCZ; and 14% and 57%, respectively, in S-ATL. Because mixing ratios of OH (the other major oxidant for  $(\text{CH}_3)_2\text{S}$ ) in the “with halogen” runs were substantially lower, these percentage contributions of halogens reflect both the enhanced oxidation by halogens and diminished oxidation by OH relative to “no halogens” runs.

## Chemical processing of inorganic halogens and related species

W. C. Keene et al.

Title Page

Abstract

Introduction

Conclusions

References

Tables

Figures

◀

▶

◀

▶

Back

Close

Full Screen / Esc

Printer-friendly Version

Interactive Discussion



Overall, the atmospheric lifetimes of  $(\text{CH}_3)_2\text{S}$  within the EURO and N-AFR regime in the “with halogens” and “no halogens” runs were similar but those with the ITCZ and S-ATL were lower by factors of 5.9 and 1.8, respectively. The oxidation of  $(\text{CH}_3)_2\text{S}$  by Cl may also influence the distribution of products with implications for aerosol nucleation, growth, and climate feedbacks (e.g., Stickel et al., 1992).

At aerosol solution pHs of 5 to 6, the aqueous-phase oxidation of S(IV) by hypohalous acids substantially accelerates production of S(VI) relative to other oxidation pathways and thereby reduces the potential for nucleation and growth of new particles and associated influences on radiative transfer (Keene et al., 1998). Because this pathway is strongly pH dependent, direct comparisons between relative rates of S oxidation in the “with halogens” versus “no halogens” runs are misleading because the influence of HCl phase partitioning on solution pH was not considered in the latter and, consequently, the low solution pHs in the “no halogens” runs (Fig. 9) are not representative. However, relative contributions of hypohalous acids to total S(IV) oxidation in the “with halogens” runs for EURO (3%), N-AFR (11%), ITCZ (39%), and S-ATL (3%) indicate that, with the exception of the ITCZ, these pathways accounted for relatively minor fractions of S(VI) production. In all regimes, scavenging of  $\text{H}_2\text{SO}_4$  vapor was the single most important pathway (Table 3). Both the measurements and simulations indicate that all aerosol size fractions in all regimes were acidic, a prerequisite for significant halogen activation and autocatalytic cycling (Keene et al., 1998). However, the effective solubility of  $\text{SO}_2$  over the range of estimated pHs (most between 3 and 4) is low (e.g., Keene et al., 1998) and, consequently, oxidation of S(IV) by hypohalous acids was relatively unimportant. The combination of relatively higher solution pHs and HOCl mixing ratios in the ITCZ regime sustained relatively greater production rates via this pathway. These results suggest that significant aqueous-phase oxidation of S(IV) by hypohalous acids may be limited spatially and temporally to a relatively narrow set of conditions in which 1) acids and acid precursors are present at sufficiently high concentrations to titrate sea-salt alkalinity (required to drive halogen-activation chemistry), 2) acids and acid precursors are present at sufficiently low concentrations such that so-

## Chemical processing of inorganic halogens and related species

W. C. Keene et al.

Title Page

Abstract

Introduction

Conclusions

References

Tables

Figures

◀

▶

◀

▶

Back

Close

Full Screen / Esc

Printer-friendly Version

Interactive Discussion



lution pHs remains above  $\sim 4.5$  (required for significant  $\text{SO}_2$  dissolution), and 3) mixing ratios of HOCl are relatively high.

Several factors influenced variability in the multiphase processing of inorganic Br and related oxidation processes. First, under conditions of moderate to low levels of pollutants (N-AFR, ITCZ, and S-ATL), both measurements and simulations indicate that most size fractions of marine aerosol were rapidly and substantially debrominated. Consequently, under these conditions, the activation flux of volatile inorganic Br varied as a function of the corresponding production flux of sea salt  $\text{Br}^-$  from the ocean surface (e.g., Fig. 7a). These results suggest that, for marine regions in which sufficient acidity is present to titrate sea-salt alkalinity and sufficient light is present to drive photochemistry, Br activation scales roughly proportionately with marine aerosol production and, thus, with the underlying physical drivers (primarily wind velocity, fetch, and sea state).

Second, in the heavily polluted EURO regime, in other polluted marine regions (e.g., Keene et al., 2007a), and to a lesser extent in less polluted regions (Fig. 2b, Sander et al., 2003), significant Br is apparently sequestered in aerosol solutions by unknown factors and, thus, not considered in current models. This was most evident in the substantial Br enrichment measured in the smallest aerosol size fractions for the EURO and N-AFR regimes, which, curiously, were not observed in the two southern regimes. Data compiled by Sander et al. (2003) also indicate a tendency for higher  $\text{EF}(\text{Br}^-)$ s for sub- $\mu\text{m}$  marine aerosols in the Northern relative to the Southern Hemispheres. In addition, the shorter-lived, super- $\mu\text{m}$  size fractions, which dominate the production flux of particulate  $\text{Br}^-$ , also retained  $\text{Br}^-$  at levels greater than predicted by the model. The retention of significant  $\text{Br}^-$  in the aerosol effectively reduces Br activation per unit sea-salt production in ambient air relative to model predictions. Consequently, the modeled mixing ratios of  $\text{Br}_t$  are considered upper limits and the corresponding influences on chemical processes in the MBL diverge from those in ambient marine air. The lower modeled versus measured  $\text{EF}(\text{Br}^-)$  also implies more efficient production of  $\text{BrCl}$  versus  $\text{Br}_2$  via hypohalous reactions with particulate halide ions in the model relative to

## Chemical processing of inorganic halogens and related species

W. C. Keene et al.

Title Page

Abstract

Introduction

Conclusions

References

Tables

Figures

◀

▶

◀

▶

Back

Close

Full Screen / Esc

Printer-friendly Version

Interactive Discussion



ambient air (Fickert et al., 1999). Because BrCl was a major precursor for atomic Cl in all regimes, the modeled concentrations of atomic Cl may also represent upper limits.

Third, at high  $\text{NO}_x$  mixing ratios in the heavily polluted EURO region, the production of halogen nitrates slowed halogen radical recycling and associated ozone destruction in the gas phase. These transformations coupled with the high levels of  $\text{NO}_x$  contributed to the relatively minor influences of halogens on conventional  $\text{HO}_x/\text{NO}_x$  chemistry under these conditions. In less polluted regions, model calculations suggest that the relative influences of Br and Cl on  $\text{O}_3$  and  $\text{NO}_x$  were substantial. In the cleanest regime (the ITCZ), simulated  $\text{NO}_x$  in the “with halogens” run was a factor of 1.9 lower relative to the “no halogens” run and the corresponding mixing ratios of OH and  $\text{HO}_2$  were also substantially lower (Table 3). Taken together, the above results suggest that, in more remote marine regions containing sufficient acidity to titrate sea-salt alkalinity, halogen chemistry significantly modifies the photochemical evolution of the MBL relative to that predicted based on conventional  $\text{HO}_x/\text{NO}_x$  chemistry.

## 4 Summary and conclusions

- The multiphase processing of inorganic Cl- and Br-species was characterized over a broad range of physiochemical conditions within four distinct flow regimes along a latitudinal gradient from  $51^\circ\text{N}$  to  $17^\circ\text{S}$  through the eastern North and South Atlantic Oceans. Median dry-deposition fluxes of sea salt, total  $\text{NO}_3$ , and total nss S among the four regimes varied by factors of 25, 17, and 9, respectively.
- Median dry-deposition fluxes of particulate and volatile Cl and Br calculated directly from measurements within each regime were approximately balanced by the corresponding production fluxes of  $\text{Cl}^-$  and  $\text{Br}^-$  in association with sea-salt aerosol. These relationships support the hypothesis that the production of sea salt at the ocean surface was the primary source for inorganic Cl and Br under all flow regimes.

## Chemical processing of inorganic halogens and related species

W. C. Keene et al.

Title Page

Abstract

Introduction

Conclusions

References

Tables

Figures

◀

▶

◀

▶

Back

Close

Full Screen / Esc

Printer-friendly Version

Interactive Discussion



**Chemical processing  
of inorganic halogens  
and related species**

W. C. Keene et al.

- 5 – Acidification and associated dechlorination of sea-salt aerosol primarily via incorporation of  $\text{HNO}_3$  sustained HCl mixing ratios ranging from median values of 82 to  $682 \text{ pmol mol}^{-1}$  (in the ITCZ and EURO regimes, respectively). Corresponding  $\text{EF}(\text{Cl}^-)$ s ranged from 0.86 to 0.94 (in the EURO and N-AFR regimes, respectively).
- 10 – Aerosol pHs inferred from the measured phase partitioning of HCl were similar to modeled values. Median pHs for most sea-salt size fractions ranged from  $\sim 3$  in the EURO regime to the low 4s in the ITCZ.
- 15 – Simulated daily maximum concentrations of atomic Cl ranged from  $2.1 \times 10^4 \text{ cm}^{-3}$  for the ITCZ to  $7.8 \times 10^4 \text{ cm}^{-3}$  for the N-AFR regime. At these levels, atomic Cl was an important oxidant for alkanes and  $(\text{CH}_3)_2\text{S}$  in all regimes. The principal sources for atomic Cl were BrCl photolysis and  $\text{ClO}+\text{NO}$ ; BrCl dominated in the three cleaner regimes and  $\text{ClO}+\text{NO}$  in the heavily polluted EURO regime.  $\text{Cl}_2$ , produced primarily at night via  $\text{HOCl}+\text{Cl}^-$ , was an important precursor only in the EURO regime. Unlike the situation in a chemically evolving (non-steady-state) pollutant plume over the ocean (e.g., Pechtl and von Glasow, 2007; Lawler et al., 2009),  $\text{Cl}_2$  recycling via autocatalytic transformations was relatively unimportant. The production and photolysis of  $\text{ClNO}_2$  was an insignificant source for atomic Cl under all conditions.
- 20 – Simulated HOCl was present in all regimes during the daytime with maximum mixing ratios ranging from 8.8 to  $51 \text{ pmol mol}^{-1}$  in the S-ATL and EURO regimes, respectively. However, the solubility of  $\text{SO}_2$  over the estimated ranges in aerosol-solution pH range was low and, consequently, oxidation of S(IV) by hypohalous acids was a relatively minor source for S(VI) in all but the ITCZ regime.
- 25 – Relative to sea salt, all individual aerosol samples integrated over particle size were significantly depleted in  $\text{Br}^-$  (median  $\text{EF}(\text{Br}^-)=0.25$ ). The highest  $\text{EF}(\text{Br}^-)$ s were in the heavily polluted EURO regime (median=0.52) and the lowest in the

Title Page

Abstract

Introduction

Conclusions

References

Tables

Figures

◀

▶

◀

▶

Back

Close

Full Screen / Esc

Printer-friendly Version

Interactive Discussion



**Chemical processing  
of inorganic halogens  
and related species**

W. C. Keene et al.

[Title Page](#)[Abstract](#)[Introduction](#)[Conclusions](#)[References](#)[Tables](#)[Figures](#)[⏪](#)[⏩](#)[◀](#)[▶](#)[Back](#)[Close](#)[Full Screen / Esc](#)[Printer-friendly Version](#)[Interactive Discussion](#)

relatively cleaner S-ATL regime (median=0.14). In contrast, simulations based on the autocatalytic halogen activation mechanism as currently understood predict almost complete debromination of the aerosol under all conditions. In addition, simulated  $Br_t$  was greater than measured mixing ratios under most conditions. These results point to an important gap in current understanding of chemical processes involving the activation and/or recycling of inorganic Br in marine air and suggest that the corresponding simulated influences of Br-radical chemistry reported herein represent upper limits.

- Reaction with atomic Br was a significant chemical sink for  $O_3$  in the N-AFR (46% of total), ITCZ (35%), and S-ATL (30%) regimes but not in the EURO regime (5%). Reaction with atomic Cl accounted for 1% to 5% of the total  $O_3$  sink in all regimes.
- The formation of halogen nitrates accelerated the oxidation of  $NO_x$  to  $HNO_3$  and particulate  $NO_3^-$  primarily via hydrolysis reactions involving S aerosol. Lower mixing ratios of  $NO_x$  coupled with direct reactions involving  $HO_x$  and halogens resulted in lower peak simulated OH concentrations during midday in the Euro (20%), N-AFR (54%), ITCZ (29%), and S-ATL (40%) regimes relative to the “no halogens” runs with implications for the lifetimes of reactive trace gases.
- Under all conditions, transformations involving halogens resulted in net  $O_3$  destruction. Relative to “no halogens” runs, average steady-state mixing ratios of  $O_3$  in the “with halogens” runs were lower by 22% in EURO, 62% in N-AFR, 29% in ITCZ, and 48% in S-ATL.
- The interrelated influences of halogens on  $NO_x$ ,  $HO_x$ , and  $O_3$  in the model substantially modified oxidation processes and atmospheric lifetimes of reactive trace gases relative to those predicted by conventional  $HO_x/NO_x$  chemistry. The relative importance of these influences varied as functions of sea-salt concentrations, absolute levels of pollutant-derived species, and the photochemical age of pollutants.

*Acknowledgements.* We thank the captain and crew of the *Polarstern* for outstanding logistical support during the cruise. Lucy Carpenter, Gordon McFiggans, Ulrich Platt and their respective post doctoral fellows, students, and technical staffs collaborated in the field campaign and shared data. Roland von Glasow provided helpful comments on the manuscript and collaborated in estimating scale heights for aerosol mixing. The Marine and Atmospheric Chemistry Research Laboratory at the University of North Carolina, Wilmington provided facilities for modeling and data interpretation. Financial support was provided by the U.S. National Science Foundation through awards ATM 0328342 and 0646854 to the University of Virginia (UVA) and ATM 0401622 and 0646865 to the University of New Hampshire (UNH) and by NOAA Contract NA03OAR4600122 to UNH. Additional support for the modeling component was provided by the U.S. Department of Energy's SciDAC Program (award DE-FG02-07ER64442 to the UVA) and Office of Biological and Environmental Research Global Change Education Program.

## References

- Alicke, B., Hebestreit, K., Stutz, J., and Platt, U.: Iodine oxide in the marine boundary layer, *Nature*, 397, 572–573, 1999.
- Bardwell, C. A., Maben, J. R., Hurt, J. A., Keene, W. C., Galloway, J. N., Boatman, J. F., and Wellman, D.: A technique using highflow, dichotomous filter packs for measuring major atmospheric chemical constituents, *Global Biogeochem. Cy.*, 4, 151–163, 1990.
- Blanchard, D. C., Woodcock, A. H., and Cipriano, R. J.: The vertical distribution of the concentration of sea salt in the marine atmosphere near Hawaii, *Tellus*, 36B, 118–125, 1984.
- Bloss, W. J., Lee, J. D., Johnson, G. P., Sommariva, R., Heard, D. E., Saiz-Lopez, A., Plane, J. M. C., McFiggans, G., Coe, H., Flynn, M., Williams, P., Rickard, A. R., and Fleming, Z. L.: Impact of halogen monoxide chemistry upon boundary layer OH and HO<sub>2</sub> concentrations at a coastal site, *Geophys. Res. Lett.*, 32, L06814, doi:10.1029/2004GL022084, 2005.
- Carpenter, L. J.: Iodine in the marine boundary layer, *Chem. Rev.*, 103, 4953–4962, 2003.
- Carsey, T. P., Churchill, D. D., Farmer, M. L., Fischer, C. J., Pszenny, A. A. P., Ross, V. B., Saltzman, E. S., Springer-Young, M., and Bonsang, B.: Nitrogen oxides and ozone production in the North Atlantic marine boundary layer, *J. Geophys. Res.*, 102, 10653–10665, 1997.
- Corbett, J. J., Fischbeck, P. S., and Pandis, S. N.: Global nitrogen and sulfur inventories for oceangoing ships, *J. Geophys. Res.*, 104, 3457–3470, 1999.

## Chemical processing of inorganic halogens and related species

W. C. Keene et al.

Title Page

Abstract

Introduction

Conclusions

References

Tables

Figures

◀

▶

◀

▶

Back

Close

Full Screen / Esc

Printer-friendly Version

Interactive Discussion



**Chemical processing  
of inorganic halogens  
and related species**

W. C. Keene et al.

[Title Page](#)[Abstract](#)[Introduction](#)[Conclusions](#)[References](#)[Tables](#)[Figures](#)[◀](#)[▶](#)[◀](#)[▶](#)[Back](#)[Close](#)[Full Screen / Esc](#)[Printer-friendly Version](#)[Interactive Discussion](#)

Dahl, E. E., Yvon-Lewis, S. A., and Saltzman, E. S.: Saturation anomalies of alkyl nitrates in the tropical Pacific Ocean, *Geophys. Res. Lett.*, 32, L20817, doi:10.1029/2005GL023896, 2005.

Dickerson, R. R., Rhoads, K. P., Carsey, T. P., Oltmans, S. J., Burrows, J. P., and Crutzen, P. J.: Ozone in the remote marine boundary layer: A possible role for halogens, *J. Geophys. Res.*, 104, 21385–21395, 1999.

Draxler, R. R. and Rolph, G. D.: HYSPLIT (Hybrid Single-Particle Lagrangian Integrated Trajectory) model access via NOAA ARL READY, NOAA Air Resources Lab., Silver Spring, MD, 2005.

Fickert, S., Adams, J. D., and Crawley, J. N.: Activation of Br<sub>2</sub> and BrCl via uptake of HOBr onto aqueous salt solutions, *J. Geophys. Res.*, 104, 23719–23727, 1999.

Finley, B. D. and Saltzman, E. S.: Measurement of Cl<sub>2</sub> in coastal urban air, *Geophys. Res. Lett.*, 33, L11809, doi:10.1029/2006GL025799, 2006.

Fischer, E., Pszenny, A., Keene, W., Maben, J., Smith, A., Stohl, A., and Talbot, R.: Nitric acid phase partitioning and cycling in the New England coastal atmosphere, *J. Geophys. Res.*, 111, D23S09, doi:10.1029/2006JD007328, 2006.

Foster, K. L., Plastridge, R. A., Bottenheim, J. W., Shepson, P. B., Finlayson-Pitts, B. J., and Spicer, C. W.: The role of Br<sub>2</sub> and BrCl in surface ozone destruction at polar sunrise, *Science*, 291, 471–474, 2001.

Galbally, I. E., Bentley, S. T., and Meyer, C. P.: Mid-latitude marine boundary-layer ozone destruction at visible sunrise observed at Cape Grim, Tasmania, *Geophys. Res. Lett.*, 27, 3841–3844, 2000.

Huebert, B. J., Zhuang, L., Howell, S., Noone, K., and Noone, B.: Sulfate, nitrate, methane-sulfonate, chloride, ammonium, and sodium measurements from ship, island, and aircraft during the Atlantic Stratocumulus Transition Experiment/Marine Aerosol Gas Exchange, *J. Geophys. Res.*, 101, 4413–4423, 1996.

Hummelshøj, P., Jensen, N. O., and Larsen, S. E.: Particle dry deposition to a sea surface, in: *Precipitation Scavenging and Atmosphere-Surface Exchange*, edited by: Schwartz, S. E. and Slinn, W. G. N., Hemisphere Publ. Corp., Washington, USA, 829–840, 1992.

Immler, F. and Schrems, O.: Lidar observations of extremely thin clouds at the tropical tropopause, *Reviewed and Revised Papers Presented at the 23rd International Laser Radar Conference*, Nara, Japan, 24–28 July 2006, edited by: Nagasawa, C. and Sugimoto, N., 547–550, 2006.

- Jacobi, H.-W., Weller, R., Bluszczyk, T., and Schrems, O.: Latitudinal distribution of peroxyacetyl nitrate (PAN) over the Atlantic Ocean, *J. Geophys. Res.*, 104(D21), 26901–26912, 1999.
- Keene, W. C., Pszenny, A. A. P., Galloway, J. N., and Hawley, M. E.: Sea-salt corrections and interpretation of constituent ratios in marine precipitation, *J. Geophys. Res.*, 91, 6647–6658, 1986.
- Keene, W. C., Talbot, R. W., Andreae, M. O., Beecher, K., Berresheim, H., Castro, M., Farmer, J. C., Galloway, J. N., Hoffmann, M. R., Li, S.-M., Maben, J. R., Munger, J. W., Norton, R. B., Pszenny, A. A. P., Puxbaum, H., Westberg, H., and Winiwarter, W.: An intercomparison of measurement systems for vapor- and particulate-phase concentrations of formic and acetic acids, *J. Geophys. Res.*, 94, 6457–6471, 1989.
- Keene, W. C., Pszenny, A. A. P., Jacob, D. J., Duce, R. A., Galloway, J. N., Schultz-Tokos, J. J., Sievering, H., and Boatman, J. F.: The geochemical cycling of reactive chlorine through the marine troposphere, *Global Biogeochem. Cy.*, 4, 407–430, 1990.
- Keene, W. C., Maben, J. R., Pszenny, A. A. P., and Galloway, J. N.: Measurement technique for inorganic chlorine gases in the marine boundary layer, *Environ. Sci. Technol.*, 27, 866–874, 1993.
- Keene, W. C., Jacob, D. J., and Fan, S.-M.: Reactive chlorine: A potential sink for dimethylsulfide and hydrocarbons in the marine boundary layer, “New Directions” Commentary, *Atmos. Environ.*, 30(6), i–iii, 1996.
- Keene, W. C., Sander, R., Pszenny, A. A. P., Vogt, R., Crutzen, P. J., and Galloway, J. N.: Aerosol pH in the marine boundary layer: A review and model evaluation, *J. Aerosol Sci.*, 29, 339–356, 1998.
- Keene, W. C., Khalil, M. A. K., Erickson, D. J., McCulloch, A., Graedel, T. E., Lobert, J. M., Aucott, M. L., Gong, S. L., Harper, D. B., Kleiman, G., Midgley, P., Moore, R. M., Seuzaret, C., Sturges, W. T., Benkovitz, C. M., Koropalov, V., Barrie, L. A., and Li, Y. F.: Composite global emissions of reactive chlorine from natural and anthropogenic sources: Reactive Chlorine Emissions Inventory, *J. Geophys. Res.*, 104, 8429–8440, 1999.
- Keene, W. C., Pszenny, A. A. P., Maben, J. R., Stevenson, E., and Wall, A.: Closure evaluation of size-resolved aerosol pH in the New England coastal atmosphere during summer, *J. Geophys. Res.*, 109, D23307, doi:10.1029/2004JD004801, 2004.
- Keene, W. C., Stutz, J., Pszenny, A. A. P., Maben, J. R., Fischer, E. V., Smith, A. M., von Glasow, R., Pechtl, S., Sive, B. C., and Varner, R. K.: Inorganic chlorine and bromine in coastal New England air during summer, *J. Geophys. Res.*, 112, D10S12, doi:10.1029/2006JD007689,

---

**Chemical processing  
of inorganic halogens  
and related species**

---

W. C. Keene et al.

---

[Title Page](#)[Abstract](#)[Introduction](#)[Conclusions](#)[References](#)[Tables](#)[Figures](#)[◀](#)[▶](#)[◀](#)[▶](#)[Back](#)[Close](#)[Full Screen / Esc](#)[Printer-friendly Version](#)[Interactive Discussion](#)

2007a.

Keene, W. C., Maring, H., Maben, J. R., Kieber, D. J., Pszenny, A. A. P., Dahl, E. E., Izaguirre, M. A., Davis, A. J., Long, M. S., Zhou, X., Smoydzin, L., and Sander, R.: Chemical and physical characteristics of nascent aerosols produced by bursting bubbles at a model air-sea interface, *J. Geophys. Res.*, 112, D21202, doi:10.1029/2007JD008464, 2007b.

Lawler, M. J., Finley, B. D., Keene, W. C., Pszenny, A. A. P., Read, K. A., von Glasow, R., and Saltzman, E. S.: Pollution-enhanced reactive chlorine chemistry in the eastern tropical Atlantic boundary layer, *Geophys. Res. Lett.*, 36, L08810, doi:10.1029/2008GL036666, 2009.

Lee, J. D., Moller, S. J., Read, K. A., Lewis, A. C., Mendes, L., and Carpenter, L.: Year round measurements of nitrogen oxides and ozone in the tropical North Atlantic marine boundary layer, *J. Geophys. Res.*, submitted, 2009.

Leser, H., Hönninger, G., and Platt U.: MAX-DOAS measurements of BrO and NO<sub>2</sub> in the marine boundary layer, *Geophys. Res. Lett.*, 30(10), 1537, doi:10.1029/2002GL015811, 2003.

Lewis, E. R. and Schwartz, S. E.: Sea salt aerosol production: Mechanisms, Methods, Measurements, and Models – A Critical Review, in *Geophysical Monograph*, 152, American Geophysical Union, Washington DC, USA, 413 pp., 2004.

Maben, J. R., Keene, W. C., Pszenny, A. A. P., and Galloway J. N.: Volatile inorganic chlorine in surface air over eastern North America, *Geophys. Res. Lett.*, 22, 3513–3516, 1995.

Maring, H., Savoie, D. L., Izaguirre, M. A., Custals, L., and Reid, J. S.: Vertical distributions of dust and sea-salt aerosols over Puerto Rico during PRIDE measured from a light aircraft, *J. Geophys. Res.*, 108, 8587, doi:10.1029/2002JD002544, 2003.

Matveev, V., Peleg, M., Rosen, D., Tov-Alper, D. S., Hebestreit, K., Stutz, J., Platt, U., Blake, D., and Luria, M.: Bromine oxide – ozone interactions over the Dead Sea, *J. Geophys. Res.*, 106, 10375–10387, 2001.

Nagao, I., Matsumoto, K., and Tanaka, H.: Sunrise ozone destruction found in the sub-tropical marine boundary layer, *Geophys. Res. Lett.*, 26, 3377–3380, 1999.

Neuman, J. A., Parrish, D. D., Trainer, M., Ryerson, T. B., Holloway, J. S., Nowak, J. B., Swanson, A., Flocke, F., Roberts, J. M., Brown, S. S., Stark, H., Sommariva, R., Stohl, A., Peltier, R., Weber, R., Wollny, A. G., Sueper, D. T., Hubler, G., and Fehsenfeld, F. C.: Reactive nitrogen transport and photochemistry in urban plumes over the North Atlantic Ocean, *J. Geophys. Res.*, 111, D23S54, doi:10.1029/2005JD007010, 2006.

O'Dowd, C. D., Jimenez, J. L., Bahreini, R., Flagan, R. C., Seinfeld, J. H., Hameri, K., Pirjola,

ACPD

9, 11889–11950, 2009

## Chemical processing of inorganic halogens and related species

W. C. Keene et al.

Title Page

Abstract

Introduction

Conclusions

References

Tables

Figures

◀

▶

◀

▶

Back

Close

Full Screen / Esc

Printer-friendly Version

Interactive Discussion



**Chemical processing  
of inorganic halogens  
and related species**

W. C. Keene et al.

[Title Page](#)[Abstract](#)[Introduction](#)[Conclusions](#)[References](#)[Tables](#)[Figures](#)[◀](#)[▶](#)[◀](#)[▶](#)[Back](#)[Close](#)[Full Screen / Esc](#)[Printer-friendly Version](#)[Interactive Discussion](#)

L., Kulmala, M., Jennings, S. G., and Hoffman, T.: Marine aerosol formation from biogenic iodine emissions, *Nature*, 417, 632–636, 2002.

Osthoff, H. D., Roberts, J. M., Ravishankara, A. R., Williams, E. J., Lerner, B. M., Sommariva, R., Bates, T. M., Coffman, D., Quinn, P. K., Dibb, J. E., Stark, H., Burkholder, J. B., Talukdar, R. K., Meagher, J., Fehsenfeld, F. C., and Brown, S. S.: High levels of nitryl chloride in the polluted subtropical marine boundary layer, *Nature Geosci.*, 1, 324–328, doi:10.1038/ngeo177, 2008.

Pechtl, S. and von Glasow, R.: Reactive chlorine in the marine boundary layer in the outflow of polluted continental air: A model study, *Geophys. Res. Lett.*, 34, L11813, doi:10.1029/2007GL029761, 2007.

Platt, U., Allan, W., and Lowe, D.: Hemispheric average Cl atom concentration from  $^{13}\text{C}/^{12}\text{C}$  ratios in atmospheric methane, *Atmos. Chem. Phys.*, 4, 2393–2399, 2004, <http://www.atmos-chem-phys.net/4/2393/2004/>.

Pszenny, A. A. P., Moldanová, J., Keene, W. C., Sander, R., Maben, J. R., Martinez, M., Crutzen, P. J., Perner, D., and Prinn, R. G.: Halogen cycling and aerosol pH in the Hawaiian marine boundary layer, *Atmos. Chem. Phys.*, 4, 147–168, 2004, <http://www.atmos-chem-phys.net/4/147/2004/>.

Pszenny, A. A. P., Fischer, E. V., Russo, R. S., Sive, B. C., and Varner, R. K.: Estimates of Cl atom concentrations and hydrocarbon kinetic reactivity in surface air at Appledore Island, Maine (USA), during International Consortium for Atmospheric Research on Transport and Transformation/Chemistry of Halogens at the Isles of Shoals, *J. Geophys. Res.*, 112, D10S13, doi:10.1029/2006JD007725, 2007.

Read, K. A., Majajan, A. S., Carpenter, L. J., Evans, M. J., Faria, B. V. E., Heard, D. E., Hopkins, J. R., Lee, J. D., Moller, S. J., Lewis, A. C., Mendes, L., McQuaid, J. B., Oetjen, H., Saiz-Lopez, A., Pilling, M. J., and Plane, J. M. C.: Extensive halogen-mediated ozone destruction over the tropical Atlantic Ocean, *Nature*, 453, 1232–1235, 2008.

Roelofs, G.-J., Lelieveld, J., and Ganzeveld, L.: Simulation of global sulfate distribution and the influence on effective cloud drop radii with a coupled photochemistry-sulfur cycle model, *Tellus*, 50b, 224–242, 1998.

Russell, L. M., Mensah, A. A., Fischer, E. V., Sive, B. C., Varner, R. K., Keene, W. C., Stutz, J., and Pszenny, A. A. P.: Nanoparticle growth following photochemical  $\alpha$ - and  $\beta$ -pinene oxidation at Appledore Island during International Consortium for Research on Transport and Transformation/Chemistry of Halogens at the Isles of Shoals 2004, *J. Geophys. Res.*,



- 112, D10S21, doi:10.1029/2006JD007736, 2007.
- Saiz-Lopez, A. and Plane, J. M. C.: Novel iodine chemistry in the marine boundary layer, *Geophys. Res. Lett.*, 31, L04112, doi:10.1029/2003GL019215, 2004.
- Saiz-Lopez, A., Plane, J. M. C., and Shillito, J. A.: Bromine oxide in the mid-latitude marine boundary layer, *Geophys. Res. Lett.*, 31, L03111, doi:10.1029/2004GL03111, 2004.
- Sander, R., Rudich, Y., von Glasow, R., and Crutzen, P. J.: The role of BrNO<sub>3</sub> in marine tropospheric chemistry: a model study, *Geophys. Res. Lett.*, 26, 2857–2860, 1999.
- Sander, R., Keene, W. C., Pszenny, A. A. P., Arimoto, R., Ayers, G. P., Baboukas, E., Caine, J. M., Crutzen, P. J., Duce, R. A., Hönninger, G., Huebert, B. J., Maenhaut, W., Mihalopoulos, N., Turekian, V. C., and Van Dingenen, R.: Inorganic bromine in the marine boundary layer: a critical review, *Atmos. Chem. Phys.*, 3, 1301–1336, 2003, <http://www.atmos-chem-phys.net/3/1301/2003/>.
- Sander, R., Kerkweg, A., Jöckel, P., and Lelieveld, J.: Technical note: The new comprehensive atmospheric chemistry module MECCA, *Atmos. Chem. Phys.*, 5, 445–450, 2005, <http://www.atmos-chem-phys.net/5/445/2005/>.
- Sandu, A. and Sander, R.: Technical note: Simulating chemical systems in Fortran90 and Matlab with the Kinetic PreProcessor KPP-2.1, *Atmos. Chem. Phys.*, 6, 187–195, 2006, <http://www.atmos-chem-phys.net/6/187/2006/>.
- Shepon, A., Gildor, H., Labrador, L. J., Butler, T., Ganzeveld, L. N., and Lawrence, M. G.: Global reactive nitrogen deposition from lightning NO<sub>x</sub>, *J. Geophys. Res.*, 112, D06304, doi:10.1029/2006JD007458, 2007.
- Simpson, W. R., von Glasow, R., Riedel, K., Anderson, P., Ariya, P., Bottenheim, J., Burrows, J., Carpenter, L. J., Frieß, U., Goodsite, M. E., Heard, D., Hutterli, M., Jacobi, H.-W., Kaleschke, L., Neff, B., Plane, J., Platt, U., Richter, A., Roscoe, H., Sander, R., Shepson, P., Sodeau, J., Steffen, A., Wagner, T., and Wolff, E.: Halogens and their role in polar boundary-layer ozone depletion, *Atmos. Chem. Phys.*, 7, 4375–4418, 2007, <http://www.atmos-chem-phys.net/7/4375/2007/>.
- Stohl, A., Forster, C., Frank, A., Seibert, P., and Wotawa, G.: Technical note: The Lagrangian particle dispersion model FLEXPART version 6.2, *Atmos. Chem. Phys.*, 5, 2461–2474, 2005, <http://www.atmos-chem-phys.net/5/2461/2005/>.
- Stickel, R. E., Nicovich, J. M., Wang, S., Zhou, Z., and Wine, P. H.: Kinetic and mechanistic study of the reaction of atomic chlorine with dimethyl sulfide, *J. Phys. Chem.*, 96, 9875–9883, 1992.

---

**Chemical processing  
of inorganic halogens  
and related species**W. C. Keene et al.

---

[Title Page](#)[Abstract](#)[Introduction](#)[Conclusions](#)[References](#)[Tables](#)[Figures](#)[◀](#)[▶](#)[◀](#)[▶](#)[Back](#)[Close](#)[Full Screen / Esc](#)[Printer-friendly Version](#)[Interactive Discussion](#)

**Chemical processing  
of inorganic halogens  
and related species**

W. C. Keene et al.

Title Page

Abstract

Introduction

Conclusions

References

Tables

Figures

◀

▶

◀

▶

Back

Close

Full Screen / Esc

Printer-friendly Version

Interactive Discussion



Stutz, J., Hebestreit, K., Alicke, B., and Platt, U.: Chemistry of halogen oxides in the troposphere: Comparison of model calculations with recent field data, *J. Atmos. Chem.*, **34**, 65–85, 1999.

Tanaka, P. L., Riemer, D. D., Chang, S., Yarwood, G., McDonald-Buller, E. C., Apel, E. C., Orlando, J. J., Silva, P. J., Jimenez, J. L., Canagaratna, M. R., Neece, J. D., Mullins, C. B., and Allen, D. T.: Direct evidence for chlorine-enhanced urban ozone formation in Houston, Texas, *Atmos. Environ.*, **37**, 1393–1400, 2003.

Thompson, A. M. and Zafiriou, O. C.: Air-sea fluxes of transient atmospheric species, *J. Geophys. Res.*, **88**, 6696–6708, 1983.

Toumi, R.: BrO as a sink for dimethylsulfide in the marine atmosphere, *Geophys. Res. Lett.*, **21**, 117–120, 1994.

Valigura, R. A.: Iterative bulk exchange model for estimating air-water transfer of HNO<sub>3</sub>, *J. Geophys. Res.*, **100**(D12) 26045–26050, 1995.

Vogt, R., Crutzen, P. J., and Sander, R.: A mechanism for halogen release from sea-salt aerosol in the remote marine boundary layer, *Nature*, **383**, 327–330, 1996.

Von Glasow R, Sander, R., Bott, A., and Crutzen, P. J.: Modeling halogen chemistry in the marine boundary layer, 1. Cloud-free MBL, *J. Geophys. Res.*, **107**, 4341, doi:10.1029/2001JD000942, 2002a.

Von Glasow, R., Sander, R., Bott, A., and Crutzen, P. J.: Modeling halogen chemistry in the marine boundary layer, 2. Interactions with sulfur and cloud-covered MBL, *J. Geophys. Res.*, **107**, 4323, doi:10.1029/2001JD000943, 2002b.

Wennberg, P. O., Cohen, R. C., Stimpfle, R. M., Koplów, J. P., Anderson, J. G., Salawitch, R. J., Fahey, D. W., Woodbridge, E. L., Keim, E. R., Gao, R. S., Webster, C. R., May, R. D., Toohey, D. W., Avallone, L. M., Proffitt, M. H., Loewenstein, M., Podolske, J. R., Chan, K. R., and Wofsy, S. C.: Removal of stratospheric O<sub>3</sub> by radicals: *In situ* measurements of OH, HO<sub>2</sub>, NO, NO<sub>2</sub>, ClO, and BrO, *Science*, **266**, 398–404, 1994.

Willeke, K.: Performance of the slotted impactor, *Amer. Indus. Hygiene Assoc. J.*, **36**, 683–691, 1975.

Williams, P. I., McFiggans, G., and Gallagher, M. W.: Latitudinal aerosol size distribution variation in the Eastern Atlantic Ocean measured aboard the FS-Polarstern, *Atmos. Chem. Phys.*, **7**, 2563–2573, 2007, <http://www.atmos-chem-phys.net/7/2563/2007/>.

Wingenter, O. W., Kubo, M. K., Blake, N. J., Smith Jr., T. W., Blake, D. R., and Rowland, F. S.:

Hydrocarbon and halocarbon measurements as photochemical and dynamical indicators of atmospheric hydroxyl, atomic chlorine and vertical mixing obtained during Lagrangian flights, J. Geophys. Res., 101, 4331–4340, 1996.

ACPD

9, 11889–11950, 2009

---

**Chemical processing  
of inorganic halogens  
and related species**

W. C. Keene et al.

---

Title Page

Abstract

Introduction

Conclusions

References

Tables

Figures

◀

▶

◀

▶

Back

Close

Full Screen / Esc

Printer-friendly Version

Interactive Discussion



## Chemical processing of inorganic halogens and related species

W. C. Keene et al.

**Table 1.** Start and stop dates, times, and positions for the four transport regimes.

	EURO	N-AFR	ITCZ	S-ATL
Start date, UTC	23 Oct	29 Oct	03 Nov	05 Nov
Start time, hh:mm UTC	06:29	07:40	07:21	18:36
Stop date, UTC	27 Oct	03 Nov	05 Nov	10 Nov
Stop time, hh:mm UTC	03:34	07:21	18:36	20:35
Start latitude, deg	51.37° N	32.79° N	9.98° N	1.36° N
Start longitude, deg	1.94° E	14.07° W	19.98° W	12.77° W
Stop latitude, deg	43.40° N	9.98° N	1.36° N	17.77° S
Stop longitude, deg	9.82° W	19.98° W	12.77° W	4.37° E

Title Page

Abstract

Introduction

Conclusions

References

Tables

Figures

◀

▶

◀

▶

Back

Close

Full Screen / Esc

Printer-friendly Version

Interactive Discussion



**Table 2.** Model parameterization.

Parameter	Units	EURO	N-AFR	ITCZ	S-ATL
Date	dd-mmm-yy	25-Oct-03	31-Oct-03	04-Nov-03	08-Nov-03
Latitude	Degrees	48° N	21° N	6° N	9° S
Temperature	°C	11.4	23.2	27.0	22.5
RH	%	56.1	67.6	78.4	77.3
Wind Velocity	m s <sup>-1</sup>	7.3	8.5	3.5	8.1
MBL Height	m	912	912	912	912
Aerosol size bins <sup>a</sup>					
Bin 1 Na <sup>+</sup> at 23 m	nmol m <sup>-3</sup>	30.4	74.0	4.4	6.8
Bin 2 Na <sup>+</sup> at 23 m	nmol m <sup>-3</sup>	45.8	132.0	7.0	12.4
Bin 3 Na <sup>+</sup> at 23 m	nmol m <sup>-3</sup>	44.3	106.0	16.1	27.9
Bin 4 Na <sup>+</sup> at 23 m	nmol m <sup>-3</sup>	12.7	42.9	11.3	21.9
Bin 5 Na <sup>+</sup> at 23 m	nmol m <sup>-3</sup>	10.9	29.7	7.7	17.0
Bin 6 Na <sup>+</sup> at 23 m	nmol m <sup>-3</sup>	3.5	9.3	1.9	4.5
Bin 7 Na <sup>+</sup> at 23 m	nmol m <sup>-3</sup>	1.4	3.2	1.8	1.3
Bin 8 nss SO <sub>4</sub> <sup>2-</sup> at 23 m	nmol m <sup>-3</sup>	15.1	13.4	8.4	9.6
Bin 1 Vertical Scaling Coeff. <sup>b</sup>		0.46	0.52	0.19	0.50
Bin 2 Vertical Scaling Coeff. <sup>b</sup>		0.79	0.82	0.61	0.81
Bin 3 Vertical Scaling Coeff. <sup>b</sup>		0.93	0.94	0.88	0.94
Bin 4 Vertical Scaling Coeff. <sup>b</sup>		0.97	0.97	0.95	0.97
Bin 5 Vertical Scaling Coeff. <sup>b</sup>		0.97	0.97	0.97	0.97
Bin 6 Vertical Scaling Coeff. <sup>b</sup>		0.97	0.97	0.97	0.97
Bin 7 Vertical Scaling Coeff. <sup>b</sup>		0.98	0.98	0.97	0.97
Bin 8 Vertical Scaling Coeff. <sup>c</sup>		1.00	1.00	1.00	1.00

## Chemical processing of inorganic halogens and related species

W. C. Keene et al.

Title Page

Abstract

Introduction

Conclusions

References

Tables

Figures

◀

▶

◀

▶

Back

Close

Full Screen / Esc

Printer-friendly Version

Interactive Discussion



**Table 2.** Continued.

Parameter	Units	EURO	N-AFR	ITCZ	S-ATL
Bin 1 Dry-Deposition Velocity	cm s <sup>-1</sup>	6.1E+000	5.7E+000	5.9E+000	5.2E+000
Bin 2 Dry-Deposition Velocity	cm s <sup>-1</sup>	2.0E+000	2.1E+000	1.4E+000	2.0E+000
Bin 3 Dry-Deposition Velocity	cm s <sup>-1</sup>	1.1E+000	1.3E+000	5.2E-001	1.2E+000
Bin 4 Dry-Deposition Velocity	cm s <sup>-1</sup>	8.9E-001	1.1E+000	3.2E-001	1.0E+000
Bin 5 Dry-Deposition Velocity	cm s <sup>-1</sup>	8.0E-001	1.0E+000	5.5E-002	9.7E-001
Bin 6 Dry-Deposition Velocity	cm s <sup>-1</sup>	1.7E-001	5.7E-001	1.9E-002	4.1E-001
Bin 7 Dry-Deposition Velocity	cm s <sup>-1</sup>	1.6E-002	2.0E-002	1.2E-002	1.8E-002
Bin 8 Dry-Deposition Velocity	cm s <sup>-1</sup>	1.6E-002	2.0E-002	1.2E-002	1.8E-002
Gas Dry-Deposition Velocity	cm s <sup>-1</sup>	1.1E+000	1.1E+000	6.8E-001	1.0E+000
O <sub>3</sub>	mol mol <sup>-1</sup>	3.5E-008	3.8E-008	2.2E-008	2.3E-008
NO <sub>2</sub> <sup>c</sup>	mol mol <sup>-1</sup>	2.0E-011	2.0E-011	2.0E-011	2.0E-011
CH <sub>4</sub> <sup>c</sup>	mol mol <sup>-1</sup>	1.8E-006	1.8E-006	1.8E-006	1.8E-006
HCHO <sup>c</sup>	mol mol <sup>-1</sup>	3.0E-010	3.0E-010	3.0E-010	3.0E-010
CO	mol mol <sup>-1</sup>	1.4E-007	1.1E-007	9.9E-008	7.7E-008
(CH <sub>3</sub> ) <sub>2</sub> S	mol mol <sup>-1</sup>	6.0E-011	6.0E-011	6.0E-011	6.0E-011
SO <sub>2</sub>	mol mol <sup>-1</sup>	3.9E-010	1.0E-010	1.9E-011	2.3E-011
H <sub>2</sub> O <sub>2</sub> <sup>c</sup>	mol mol <sup>-1</sup>	6.0E-010	6.0E-010	6.0E-010	6.0E-010
NH <sub>3</sub>	mol mol <sup>-1</sup>	2.7E-010	9.9E-011	7.7E-011	5.0E-011
HNO <sub>3</sub>	mol mol <sup>-1</sup>	2.1E-010	1.9E-011	1.2E-011	2.1E-011
HCl	mol mol <sup>-1</sup>	6.8E-010	3.5E-010	8.2E-011	2.7E-010
CH <sub>3</sub> OH <sup>c</sup>	mol mol <sup>-1</sup>	3.0E-010	3.0E-010	3.0E-010	3.0E-010

Unless otherwise noted, parameterizations correspond to median values based on data from the cruise.

<sup>a</sup> The ambient geometric mean diameters for aerosol size bins 1 through 8 were 28.8, 15.2, 7.08, 3.32, 1.75, 0.89, 0.46, and 0.18 μm, respectively.

<sup>b</sup> Based on Lewis and Schwartz (2004) (see text).

<sup>c</sup> Assumed value.

Scientific notation refers to the power 10; for example, 3.0E-010 is 3.0×10<sup>-10</sup>.

## Chemical processing of inorganic halogens and related species

W. C. Keene et al.

Title Page

Abstract

Introduction

Conclusions

References

Tables

Figures

◀

▶

◀

▶

Back

Close

Full Screen / Esc

Printer-friendly Version

Interactive Discussion



**Table 3.** Summary of selected simulated results.

	EURO <sup>a</sup>	N-AFR <sup>a</sup>	ITCZ <sup>a</sup>	S-ATL <sup>a</sup>
Cl* (24-h mean), pmol mol <sup>-1</sup>	78	19	26	14
HOCl (daytime max), pmol mol <sup>-1</sup>	51	11	21	8.8
ClNO <sub>3</sub> (daytime max), pmol mol <sup>-1</sup>	21	1.8	2.2	0.9
Cl <sub>2</sub> (nighttime, max), pmol mol <sup>-1</sup>	36	2.8	5.3	2.0
BrCl (nighttime, max), pmol mol <sup>-1</sup>	15	16	7.0	10
Cl-atom conc. (daytime max), cm <sup>-3</sup>	4.3×10 <sup>4</sup>	7.8×10 <sup>4</sup>	2.1×10 <sup>4</sup>	4.1×10 <sup>4</sup>
Sources for atomic Cl				
ClO+NO, %	36	24	16	22
BrCl photolysis, %	25	66	62	64
Cl <sub>2</sub> photolysis, %	24	3	7	1
HOCl photolysis, %	12	6	15	11
Br <sub>t</sub> (24-h mean), pmol mol <sup>-1</sup>	15	37	8.3	23
BrNO <sub>3</sub> (daytime max), pmol mol <sup>-1</sup>	14	18	3.2	9.5
HOBr (daytime max), pmol mol <sup>-1</sup>	2.5	11	3.2	7.4
HBr (daytime max), pmol mol <sup>-1</sup>	1.6	18	1.2	12
BrO (daytime max), pmol mol <sup>-1</sup>	1.0	7.8	3.0	6.5
BrCl (nighttime max), pmol mol <sup>-1</sup>	15	16	7.0	10
Br <sub>2</sub> (nighttime max), pmol mol <sup>-1</sup>	1.0	13	0.7	6.9
Sources for atomic Br				
BrO+NO, %	50	31	15	26
BrCl photolysis, %	26	18	38	19
HOBr photolysis, %	10	19	24	29
Br <sub>2</sub> photolysis, %	<1	21	7	16

## Chemical processing of inorganic halogens and related species

W. C. Keene et al.

Title Page

Abstract

Introduction

Conclusions

References

Tables

Figures

◀

▶

◀

▶

Back

Close

Full Screen / Esc

Printer-friendly Version

Interactive Discussion



**Table 3.** Continued.

	EURO <sup>a</sup>	N-AFR <sup>a</sup>	ITCZ <sup>a</sup>	S-ATL <sup>a</sup>
NO <sub>x</sub> (24-h mean), pmol mol <sup>-1</sup>	171	31	8.3	20
NO <sub>x</sub> (24-h mean, "no halogens"), pmol mol <sup>-1</sup>	237	62	27	37
NO (daytime max), pmol mol <sup>-1</sup>	28	10	1.7	7.6
NO (daytime max, "no halogens"), pmol mol <sup>-1</sup>	42	16	6.0	12
Heterogeneous NO <sub>x</sub> sinks				
S aerosol, % heterogeneous	91	69	86	79
ClNO <sub>3</sub> hydrolysis, % heterogeneous	53	14	54	16
BrNO <sub>3</sub> hydrolysis, % heterogeneous	27	54	33	59
N <sub>2</sub> O <sub>5</sub> hydrolysis, % heterogeneous	11	<1	<1	<1
BrNO <sub>3</sub> + Cl <sup>-</sup> , % heterogeneous	3	19	3	12
OH (daytime max), pmol mol <sup>-1</sup>	0.11	0.10	0.022	0.15
OH (daytime max, "no halogens"), pmol mol <sup>-1</sup>	0.13	0.22	0.031	0.25
HO <sub>2</sub> (daytime max), pmol mol <sup>-1</sup>	9.2	12	4.4	14
HO <sub>2</sub> (daytime max, "no halogens"), pmol mol <sup>-1</sup>	8.2	17	6.0	18
O <sub>3</sub> (24-h mean), nmol mol <sup>-1</sup>	49	14	29	14
O <sub>3</sub> (24-h mean, "no halogen"), nmol mol <sup>-1</sup>	64	37	41	28
O <sub>3</sub> chemical sinks				
O <sub>3</sub> +Br, %	5	46	35	30
O <sub>3</sub> +Cl, %	3	2	5	1
Sources for particulate nss SO <sub>4</sub> <sup>2-</sup>				
H <sub>2</sub> SO <sub>4</sub> scavenging, %	96	81	50	92
HOCl+S(IV), %	3	11	39	3

<sup>a</sup>Unless otherwise noted, results correspond to "with halogens" runs.

## Chemical processing of inorganic halogens and related species

W. C. Keene et al.

Title Page

Abstract

Introduction

Conclusions

References

Tables

Figures

◀

▶

◀

▶

Back

Close

Full Screen / Esc

Printer-friendly Version

Interactive Discussion



**Chemical processing  
of inorganic halogens  
and related species**

W. C. Keene et al.

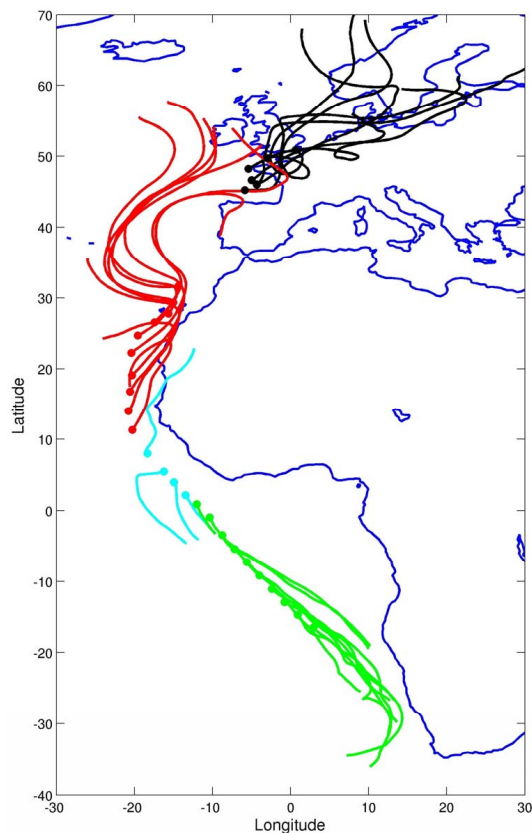


**Fig. 1.** Five-day HYSPLIT back trajectories initiated at 500-m elevation along the cruise track. Start times correspond to the midpoint of each aerosol and filter-pack sampling interval. Trajectories for the EURO regime are plotted in black, N-AFR in red, ITCZ in light blue, and S-ATL in green.

[Title Page](#)[Abstract](#)[Introduction](#)[Conclusions](#)[References](#)[Tables](#)[Figures](#)[◀](#)[▶](#)[◀](#)[▶](#)[Back](#)[Close](#)[Full Screen / Esc](#)[Printer-friendly Version](#)[Interactive Discussion](#)

Chemical processing  
of inorganic halogens  
and related species

W. C. Keene et al.

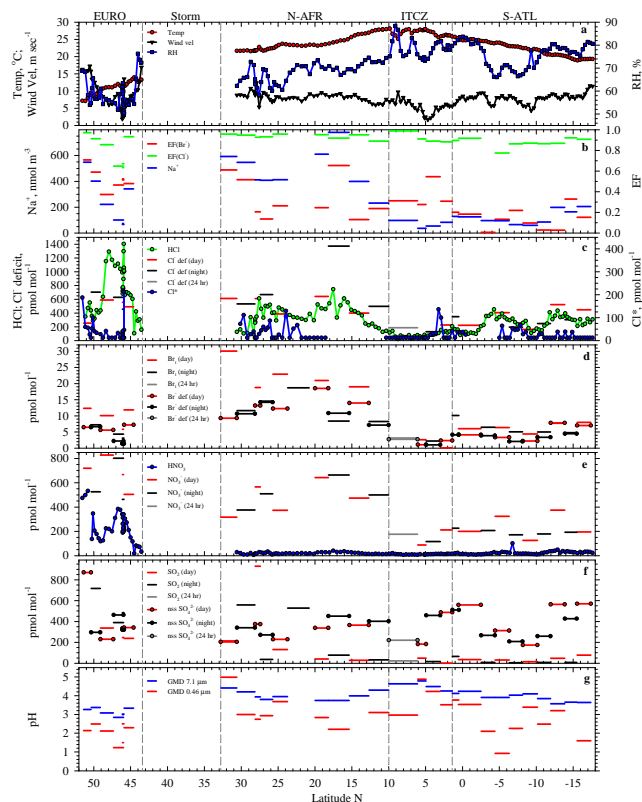


**Fig. 2.** Latitudinal variability in **(a)** air temperature, RH, and wind velocity averaged over each mist-chamber sampling interval; **(b)** particulate Na<sup>+</sup>, EF(Cl<sup>-</sup>), and EF(Br<sup>-</sup>); **(c)** HCl, Cl<sup>-</sup>, and particulate Cl<sup>-</sup> deficit; **(d)** Br<sub>t</sub> and particulate Br<sup>-</sup> deficit; **(e)** HNO<sub>3</sub> and particulate NO<sub>3</sub><sup>-</sup>; **(f)** SO<sub>2</sub> and particulate nss SO<sub>4</sub><sup>2-</sup>; and **(g)** pH of GMD 7.1-μm and GMD 0.46-μm aerosol size fractions. In panel **(f)**, SO<sub>2</sub> during the first sampling interval (2277 pmol mol<sup>-1</sup>) is off scale. Values below DLs are plotted as 0.5×DLs. Vertical dashed lines partition major transport regimes.

Title Page

Abstract

Introduction

Conclusions

References

Tables

Figures



Back

Close

Full Screen / Esc

Printer-friendly Version

Interactive Discussion



Chemical processing  
of inorganic halogens  
and related species

W. C. Keene et al.

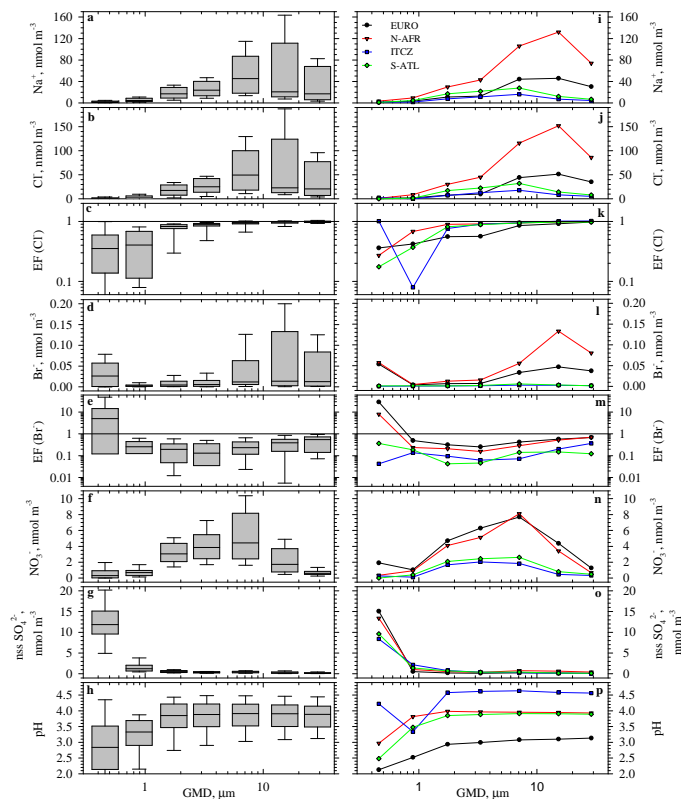


**Fig. 3.** Box and whisker plots depicting particulate size distributions (90th, 75th, 50th, 25th, and 10th percentiles) based on all data for (a)  $\text{Na}^+$ , (b)  $\text{Cl}^-$ , (c) EF( $\text{Cl}^-$ ), (d)  $\text{Br}^-$ , (e) EF( $\text{Br}^-$ ), (f)  $\text{NO}_3^-$ , (g) nss  $\text{SO}_4^{2-}$ , and (h) aerosol pH. Median size distributions of (i)  $\text{Na}^+$ , (j)  $\text{Cl}^-$ , (k) EF( $\text{Cl}^-$ ), (l)  $\text{Br}^-$ , (m) EF( $\text{Br}^-$ ), (n)  $\text{NO}_3^-$ , (o) nss  $\text{SO}_4^{2-}$ , and (p) aerosol pH for each transport regime.

Title Page

Abstract

Introduction

Conclusions

References

Tables

Figures

◀

▶

◀

▶

Back

Close

Full Screen / Esc

Printer-friendly Version

Interactive Discussion



Chemical processing  
of inorganic halogens  
and related species

W. C. Keene et al.

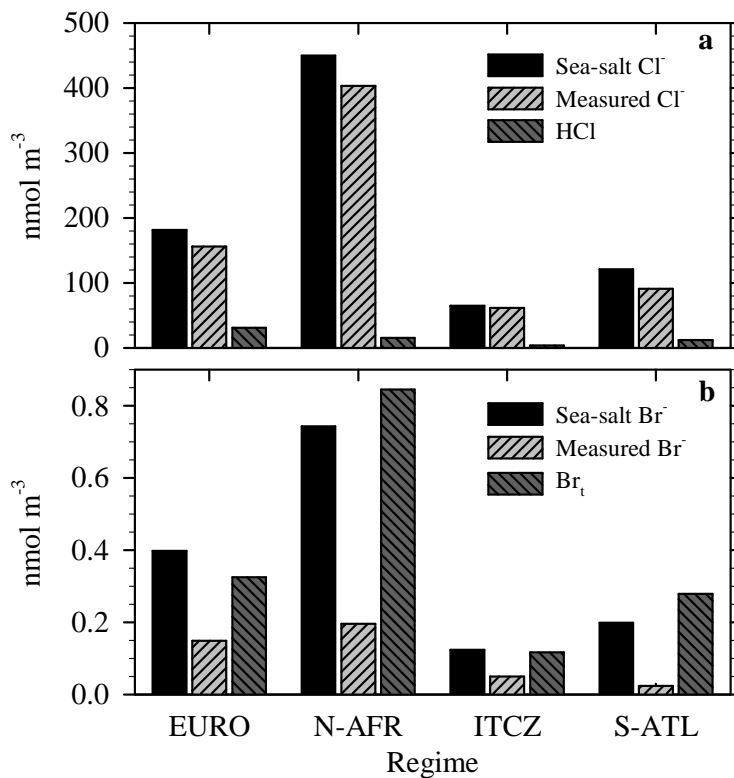


**Fig. 4.** Median concentrations of (a)  $\text{ss Cl}^-$ , measured  $\text{Cl}^-$ , and HCl, (b)  $\text{ss Br}^-$ , measured  $\text{Br}^-$ , and volatile inorganic Br for each regime.

[Title Page](#)[Abstract](#)[Introduction](#)[Conclusions](#)[References](#)[Tables](#)[Figures](#)[◀](#)[▶](#)[◀](#)[▶](#)[Back](#)[Close](#)[Full Screen / Esc](#)[Printer-friendly Version](#)[Interactive Discussion](#)

Chemical processing  
of inorganic halogens  
and related species

W. C. Keene et al.

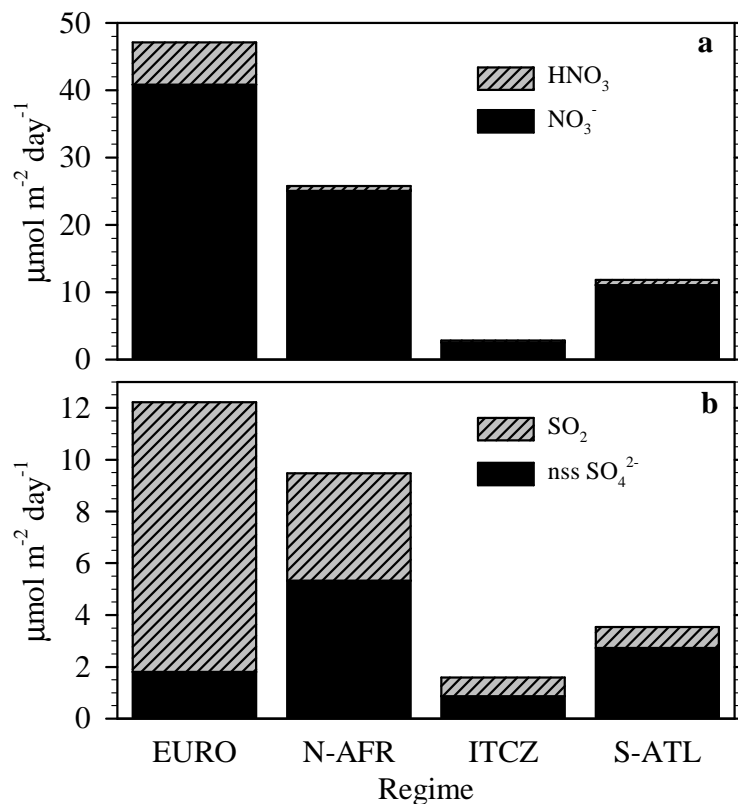


**Fig. 5.** Median dry-deposition fluxes of (a)  $\text{HNO}_3$  and particulate  $\text{NO}_3^-$ , and (b)  $\text{SO}_2$  and particulate  $\text{nss SO}_4^{2-}$  for each regime.

[Title Page](#)[Abstract](#)[Introduction](#)[Conclusions](#)[References](#)[Tables](#)[Figures](#)[◀](#)[▶](#)[◀](#)[▶](#)[Back](#)[Close](#)[Full Screen / Esc](#)[Printer-friendly Version](#)[Interactive Discussion](#)

## Chemical processing of inorganic halogens and related species

W. C. Keene et al.

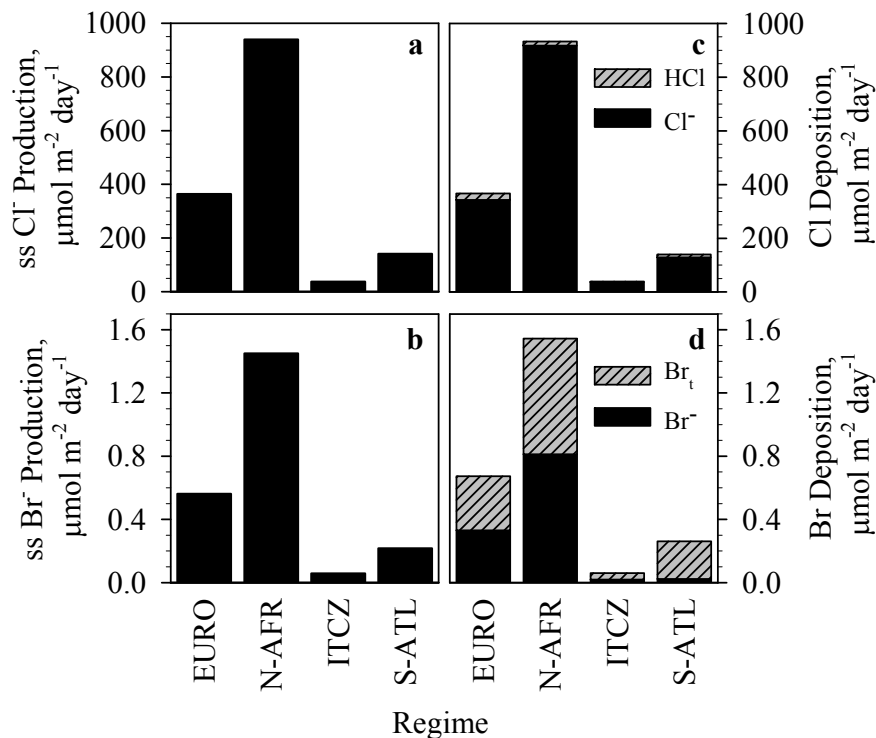


**Fig. 6.** Median emission fluxes of (a) sea-salt Cl<sup>-</sup> and (b) sea-salt Br<sup>-</sup> inferred from dry-deposition fluxes of particulate Na<sup>+</sup> versus median dry-deposition fluxes of (c) HCl and particulate Cl<sup>-</sup>, and (d) Br<sub>r</sub> and particulate Br<sup>-</sup> for each regime.

Title Page

Abstract

Introduction

Conclusions

References

Tables

Figures

◀

▶

◀

▶

Back

Close

Full Screen / Esc

Printer-friendly Version

Interactive Discussion



## Chemical processing of inorganic halogens and related species

W. C. Keene et al.

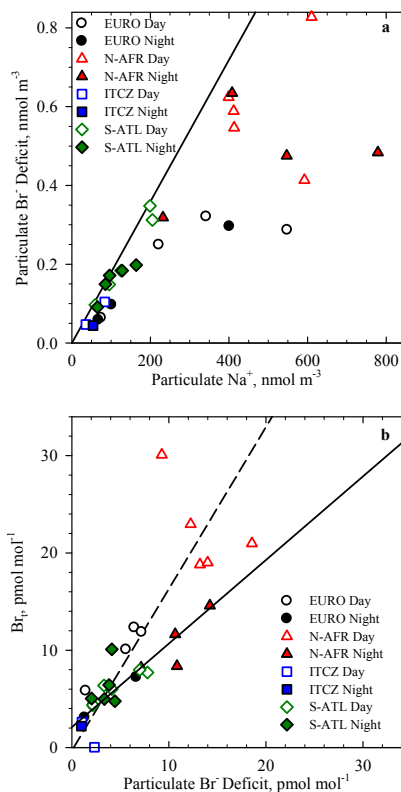


**Fig. 7.** (a) Absolute particulate  $\text{Br}^-$  deficit relative to sea salt versus particulate  $\text{Na}^+$  within the four regimes. The line depicts the ratio of particulate  $\text{Br}^-$  to  $\text{Na}^+$  in seawater ( $0.001798 \text{ mol mol}^{-1}$ ). (b)  $\text{Br}_t$  versus absolute particulate  $\text{Br}^-$  deficit relative to sea salt within the four regimes. Lines depict reduced major axis regressions (Keene et al., 1986) for daytime (dashed, slope=1.66, Y intercept=-0.3, and  $r^2=0.64$ ) and nighttime (solid, slope=0.88, Y intercept=2.1, and  $r^2=0.77$ ).

Title Page

Abstract

Introduction

Conclusions

References

Tables

Figures

◀

▶

◀

▶

Back

Close

Full Screen / Esc

Printer-friendly Version

Interactive Discussion



## Chemical processing of inorganic halogens and related species

W. C. Keene et al.

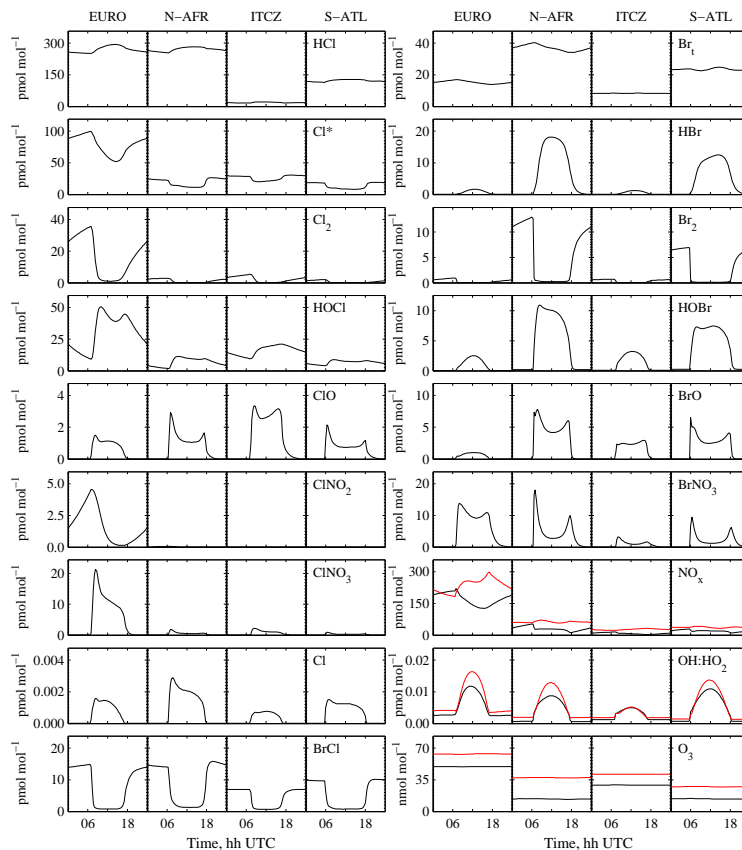


**Fig. 8.** Diel cycles in mixing ratios of gas-phase species simulated for the four flow regimes; values for runs “with halogens” are in black and those with “no halogens” are in red.

Title Page

Abstract

Introduction

Conclusions

References

Tables

Figures

◀

▶

◀

▶

Back

Close

Full Screen / Esc

Printer-friendly Version

Interactive Discussion



Chemical processing  
of inorganic halogens  
and related species

W. C. Keene et al.

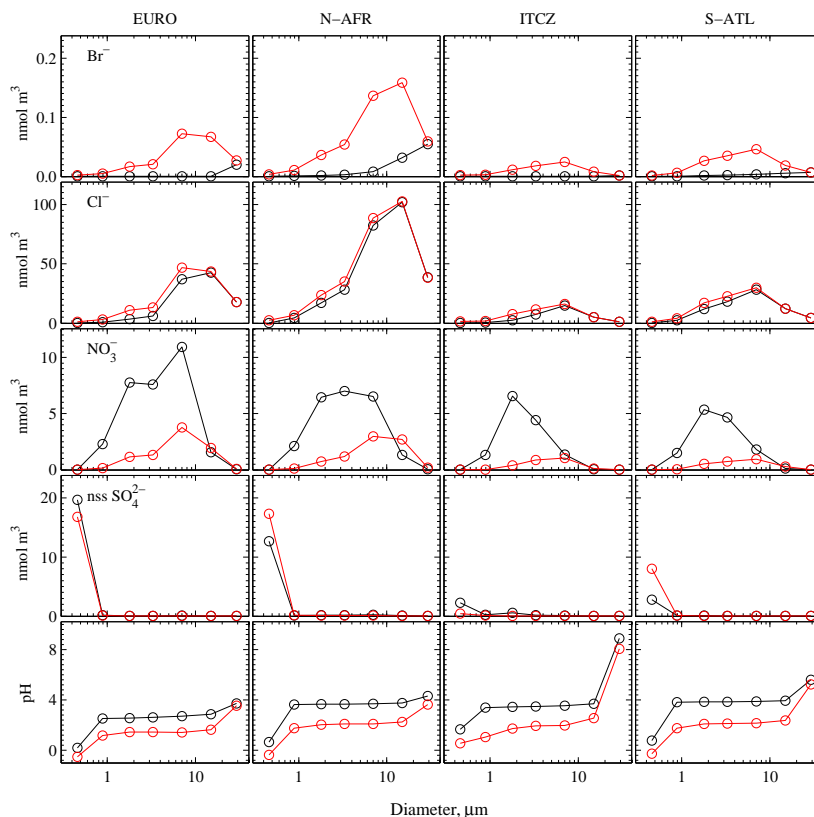


**Fig. 9.** Average size distributions of particulate-phase species simulated for the four flow regimes; values for runs “with halogens” are in black and those with “no halogens” are in red. To facilitate direct comparison with measured size distributions, constituents associated with the S size bin have been added to those associated with the smallest sea-salt size bin.

[Title Page](#)[Abstract](#)[Introduction](#)[Conclusions](#)[References](#)[Tables](#)[Figures](#)[◀](#)[▶](#)[◀](#)[▶](#)[Back](#)[Close](#)[Full Screen / Esc](#)[Printer-friendly Version](#)[Interactive Discussion](#)

## Chemical processing of inorganic halogens and related species

W. C. Keene et al.

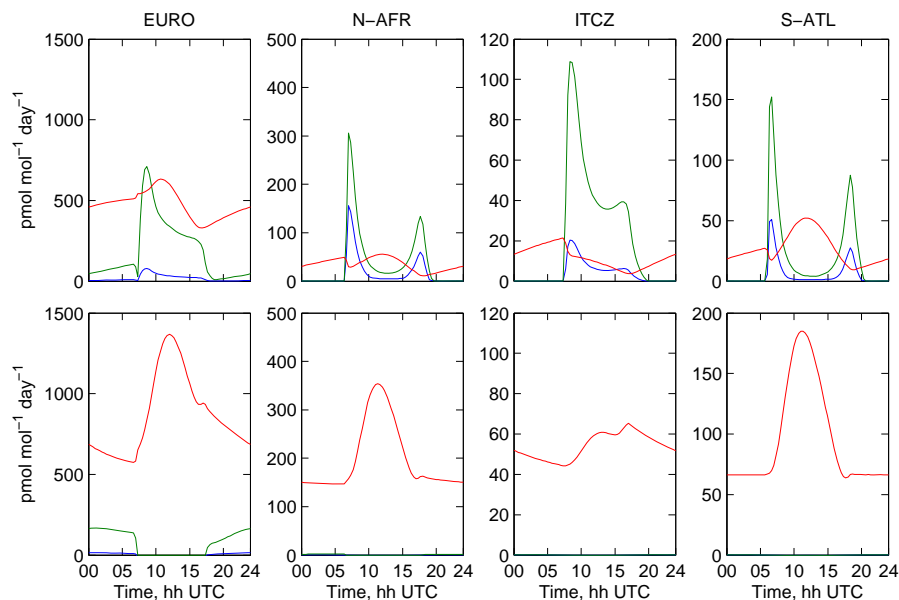


**Fig. 10.** Diel cycles in selected  $\text{NO}_x$  sinks simulated for the four flow regimes. Values for runs “with halogens” are depicted in the top row of panels and those for “no halogens” are in the bottom row. Gas-phase sinks are in red, heterogeneous reactions involving sea salt are in blue, and those involving S aerosol are in green. Gas-phase reactions include  $\text{NO}_2 + \text{O}_3$ ,  $\text{NO}_2 + \text{OH}$ , and  $\text{NO}_3 + (\text{CH}_3)_2\text{S}$ ;  $\text{HNO}_3$  photolysis is evaluated as a negative sink. Heterogeneous pathways include hydrolysis and reactions with particulate  $\text{Cl}^-$  and  $\text{Br}^-$  involving  $\text{ClNO}_3$ ,  $\text{BrNO}_3$ , and  $\text{N}_2\text{O}_5$ .

Title Page

Abstract

Introduction

Conclusions

References

Tables

Figures

◀

▶

◀

▶

Back

Close

Full Screen / Esc

Printer-friendly Version

Interactive Discussion

